J Mater Sci (2007) 42:1202–1227
DOI 10.1007/s10853-006-0094-8

Thermal stresses and related phenomena in composite ceramics

Ladislav Ceniga

Received: 25 January 2005 / Accepted: 30 March 2006 / Published online: 24 January 2007

Abstract The paper deals with elastic thermal stresses in an isotropic multi-particle-matrix system consisted of periodically distributed spherical particles in an infinite matrix, imaginarily divided into cubic cells containing a central spherical particle. Originating during a cooling process as a consequence of the difference in thermal expansion coefficients between the matrix and the particle, and investigated within the cubic cell, the thermal stresses, as functions of the particle volume fraction v, being transformed for $v = 0$ to those of an isotropic one-particle-matrix system, are maximal at the critical particle volume fraction, representing a considerable value related to maximal resistance of the thermal-stress strengthened multi-particle-matrix system against mechanical loading. The thermal stresses are derived for such temperature range within which the multi-particle-matrix system exhibits elastic deformations, considering the yield stress and the particle-matrix boundary adhesion strength. With regard to a curve integral of the thermal-stress induced elastic energy density, critical particle radii related to crack initiation in ideal-brittle particle and matrix, functions describing crack shapes in a plane perpendicular to the direction of crack formation in the particle and in the matrix, and consequently dimensions of a crack in the particle and in the matrix are derived along with the condition concerning the direction of the crack formation. Additionally, derived by two equivalent mathematical techniques, the elastic energy gradient within the cubic cell, representing a surface integral of the thermal-stress induced elastic energy density, is presented to derive the thermal-stress induced strengthening in the spherical particle and in the cubic cell matrix. The former parameters for $v = 0$ are derived using the model of a spherical cell with the radius $R_c \to \infty$. Derived formulae are applied to the SiC–Si_3N_4 multi-particle-matrix system, and calculated values of investigated parameters are in a good agreement with those from published experimental results.

L. Ceniga (✉)
Institute of Materials Research, Slovak Academy of Sciences, Watsonova 47, 043 53 Košice, Slovak Republic
e-mails: lceniga@imr.saske.sk; ceniga@post.sk; lceniga@yahoo.com

Introduction

Investigated usually by approximate computational and experimental methods [1], thermal stresses represent an important phenomenon observed in materials. With regard to material science, thermal stresses originate in a composite material as a consequence of the difference in thermal expansion coefficients between individual material components, consequently influencing mechanical properties [2, 3], superconductivity [4, 5], diffusion processes [6, 7] and consequently grain growth [8–10].

On one hand, representing resistance against mechanical loading, regarding a multi-particle-matrix system, thermal stresses depend on the particle volume fraction v of a strengthening phase (a precipitate) of the composite material, and accordingly are maximal at the critical particle volume fraction, representing a considerable value related to maximal resistance of the thermal-stress strengthened multi-particle-matrix

system [2, 3]. On the other hand, as a consequence of the particle radius R greater than critical, the thermal-stress induced energy depends on both the particle volume fraction and the particle radius, and tends to release by crack formation in a particle or in a matrix [4, 5], as dependent on the difference in thermal expansion coefficients between the material components.

The thermal stresses as functions of a position given by the coordinate x_1 induce the x_1-dependent energy density w accumulated in an arbitrary point in the composite material. As presented in this paper, the 'curve' energy density W_c as an integral of w along a curve in the composite material, representing a function of the variable x_1, is required for the determination of conditions of crack initiation and formation.

Neglecting a redistribution of the thermal stresses during high-speed crack formation, the crack formation analysed in this paper is accordingly related to brittle particle and matrix.

Additionally, included in the potential energy gradient W_p, the x_1-dependent gradient W_s, representing an energy barrier with the maximal value W_{smax} and simultaneously 'surface' energy density as an integral of w over the surface S in the composite material, influences the coercivity of magnetic materials as well as magnetic domain and dislocation structure [11].

As an example, a planar magnetic domain wall with the normal x_1, representing a front between magnetic domains with and without ordered magnetic moments, is shifted in a magnetic material along the axis x_1 from the position $x_1 = a$ to the position $x_1 = b$ by the change $\Delta H_{ba} = H_b - H_a$ of the magnetic field intensity H, where the position $x_1 = b$ correspond to a local maximum in the point B of the middle energy barrier as presented in Fig. 1. Consequently, the magnetic domain wall moves along the axis x_1 to the position $x_1 = c$ at the constant intensity $H_b = H_c$, being stopped by the third energy barrier higher than the second one. The position change of the magnetic domain wall results in the change ΔM of the magnetic moment M of the magnetic material. Accordingly, the magnetic moment change ΔM_{ba} related to the position change $\Delta x = c - b$ at $\Delta H_{cb} = H_c - H_b$ results in a discrete change of the magnetization hysteresis loop, inducing a voltage impulse in a pickup coil known as the Barkhausen jump. The change ΔH_{ba} and the $W_p - x_1$ dependence, including the $W_s - x_1$ function, are reasons of the coercivity of the magnetic material [11].

Considering the thermal-stress induced energy W accumulated in the volume V of the solid continuum of a general shape as presented in Fig. 2 in the form

$$W = \int_V w \, \mathrm{d}V = \int \int_S w \, \mathrm{d}S \, \mathrm{d}x, \tag{1}$$

the parameter W_s, derived as

$$W_s = \frac{\partial W}{\partial x} = \int_S w \, \mathrm{d}S, \tag{2}$$

represents the energy gradient along the axis x_1, equal to the 'surface' elastic energy density related to the surface S perpendicular to the axis x_1.

Additionally, the gradient W_s is required to derive thermal-stress induced micro- and macro-strengthening in the spherical particle and in the cell matrix representing material components of the composite material of a precipitate-matrix type.

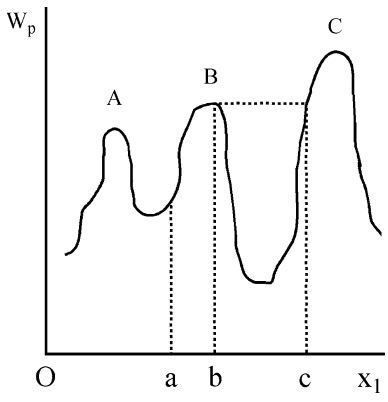

Fig. 1 The energy barriers A, B, C of the potential energy gradient W_p as a dependence on the position x_1 in a composite material. The energy barrier B exhibits the maximum for $x_1 = b$

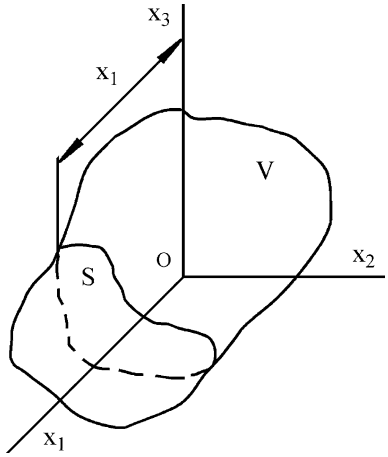

Fig. 2 The solid continuum of a general shape with the volume V, the surface $S \perp x_1$ and the Cartesian system $(Ox_1x_2x_3)$

Cell model

As an imagination considered for an analytical modelling, the composite material of the precipitate-matrix type characterized by aperiodically distributed precipitates with general shapes embedded in a matrix with finite dimensions consisted of grains is replaced by a system consisted of periodically distributed spherical particles embedded in an infinite matrix, neglecting grain boundaries. To derive the thermal stresses acting in the model system, the multi-particle-matrix system is *imaginarily* divided into identical cells with the shape to depend on a particle distribution, and accordingly the cell represents a part of the multi-particle-matrix system related to one spherical particle. Consequently, the thermal stresses are investigated within the cell, and derived formulae are valid for any cell of the infinite matrix [12–14].

Unfortunately, mathematical techniques to derive the elastic thermal stresses in an isotropic multi-particle-matrix system, i.e. in a system with isotropic components, lead to two mutually incompatible analytical models. On the one hand, formulae for thermal stresses of the first model related to an isotropic multi-particle-matrix system, as presented in [13], are transformable, on the condition of the particle volume fraction $v = 0$, to those related to an isotropic one-particle-matrix system, as presented in [15]. On the other hand, a geometrical condition represented by zero radial displacement on a cell surface, as presented in [14], and accordingly shear thermal stresses and strains are not considered within the first analytical model. Conversely, the second analytical model related to an isotropic multi-particle-matrix system, as presented in [14], including formulae for radial, tangential and shear thermal stresses and strains, non-transformable on the condition $v = 0$ to those related to an isotropic one-particle-matrix system, considers the condition of zero radial displacement on a cell surface.

Resulting from the particles distribution as presented in Fig. 3, the infinite matrix is imaginarily divided into cubic cells with the dimension d, representing an inter-particle distance, and consequently the particle volume fraction v of the multi-particle-matrix system, as the ratio of the spherical particle volume $V_p = 4\pi R^3/3$ to the cubic cell volume $V_c = d^3$, is derived as [13]

$$v = \frac{V_p}{V_c} = \frac{4\pi}{3}\left(\frac{R}{d}\right)^3 \in \left(0, \frac{\pi}{6}\right), \tag{3}$$

where $\pi/6$ results from $d = 2R$.

Due to the isotropy of the multi-particle-matrix system, the shape symmetry of the spherical particle and the cubic cell, the symmetrical distribution of the cubic cells resulting from the matrix infinity, the thermal stresses are accordingly sufficient to be investigated within one twenty-fourth of the cubic cell (see Fig. 4), then for $r \in \langle 0, r_c\rangle$, $\varphi \in \langle 0, \pi/4\rangle$, $v \in \langle v_{34}, \pi/2\rangle$, where $r_c = |OC|$, $v_{34} = \angle(x_2, OC_{34})$, C is an arbitrary point on the cubic cell surface $C_1C_2C_3C_4$, and then [13]

$$r_c = \frac{d}{2\cos\varphi \sin v}, \tag{4}$$

$$v_{34} = \arctan\left(\frac{|OC_{12}|}{|C_{12}C_{34}|}\right) = \arctan\left(\frac{1}{\cos\varphi}\right). \tag{5}$$

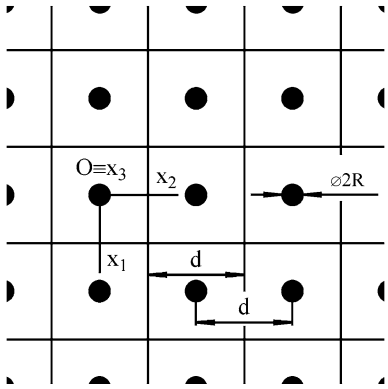

Fig. 3 The multi-particle-matrix system consisted of the periodically distributed spherical particles with the radius R, embedded in the infinite matrix imaginarily divided into the cubic cells with the dimension d, representing an inter-particle distance, and the Cartesian system $(Ox_1x_2x_3)$ in the point O in the spherical particle centre

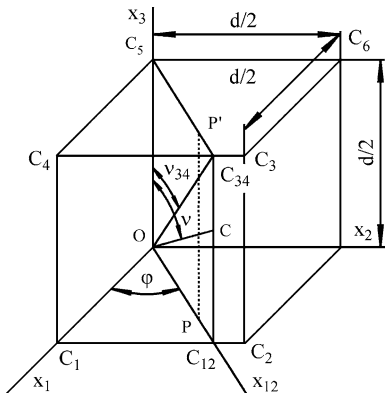

Fig. 4 The surface $C_1C_2C_3C_4$ of one-eighth of the cubic cell, the arbitrary point C on the surface $C_1C_2C_3C_4$ with the position determined by the coordinates (r_c, φ, v), and the points P, P' in the planes x_1x_2, $C_3C_4C_5C_6$, respectively, where $r_c = |OC|$, $|PP'| = d/2$, O is the spherical particle centre, d is the cubic cell dimension (see Fig. 3). The thermal stresses are sufficient to be investigated within one twenty-fourth of the cubic cell, then for $r \in \langle R, r_c\rangle$, $\varphi \in \langle 0, \pi/4\rangle$, $v \in \langle v_{34}, \pi/2\rangle$

Resulting from the first model [13], this paper presents derivations of the elastic energy density w_q in the spherical particle ($q = p$) and in the cell matrix ($q = m$), and consequently the 'curve' and 'surface' elastic energy density, W_c and W_s, respectively, regarding an elastic solid continuum represented by the cubic cell with the central spherical particle. Considering the isotropy of the multi-particle-matrix system, the cubic cell is assumed to exhibit identical circular cracks created in the planes x_1x_2, x_1x_3, x_2x_3. As presented below in detail, the determination of the crack formation conditions considers the energy $\mathrm{d}W$ accumulated in the infinitesimal volume $\mathrm{d}V$ of an infinitesimal prism with the height $PP' = d/2$ and with the surface area $\mathrm{d}S = x_{12}\,\mathrm{d}\varphi\,\mathrm{d}x_{12}$ of a basis in the plane x_1x_2 in the position $x_{12} \in \langle 0, |OC_{12}| \rangle$ along the axis $x_{12} \subset x_1x_2$ (see Fig. 4). Consequently, we get

$$\mathrm{d}W = \frac{1}{3}\int_V w\,\mathrm{d}V = \frac{\mathrm{d}S}{3}\int_P^{P'} w\,\mathrm{d}x_3 = \frac{1}{3}\,W_c x_{12}\,\mathrm{d}x_{12}\,\mathrm{d}\varphi, \tag{6}$$

and the x_{12}-dependent 'curve' elastic energy density W_{c1} and W_{c2} in the intervals $x_{12} \in \langle 0, R \rangle$ and $x_{12} \in \langle R, |OC_{12}| \rangle$, respectively, is derived as

$$W_{c1} = \int_P^{P''} w_p\,\mathrm{d}x_3 + \int_{P''}^{P'} w_m\,\mathrm{d}x_3, \quad x_{12} \in \langle 0, R \rangle, \tag{7}$$

$$W_{c2} = \int_P^{P'} w_m\,\mathrm{d}x_3, \quad x_{12} \in \langle R, |OC_{12}| \rangle, \tag{8}$$

where P'' is a point of intersection of the particle surface with the abscissa $PP' \parallel x_3$ for $x_{12} \in \langle 0, R \rangle$.

Similarly, considering one-eighth of the cubic cell, the x_1-dependent 'surface' elastic energy density W_{s1} and W_{s2} in the intervals $x_1 \in \langle 0, R \rangle$ and $x_1 \in \langle R, d/2 \rangle$ (see Fig. 5), respectively, is derived as

$$W_{s1} = 4\left(\int_{S_p} w_p\,\mathrm{d}S_p + \int_{S_m} w_m\,\mathrm{d}S_m\right), \quad x_1 \in \langle 0, R \rangle, \tag{9}$$

$$W_{s2} = 4\int_{S_m} w_m\,\mathrm{d}S_m, \quad x_1 \in \langle R, d/2 \rangle, \tag{10}$$

where the surface S_q is a part of the square surface $S_1S_2S_3S_4 \perp x_1$ related to the spherical particle ($q = p$) and to the cell matrix ($q = m$) for $x_1 \in \langle 0, R \rangle$, and $S_m \equiv S_1S_2S_3S_4$ for $x_1 \in \langle R, d/2 \rangle$.

With regard to the section 'Theoretical background' representing a contribution to the first analytical model presented in [13], this paper is accordingly suitable for material scientists to be able to determine thermal-stress loading including the thermal-stress induced strengthening and the conditions of crack initiation related to the spherical particle and to the cell matrix as material components of the precipitate-matrix type. With regard to the crack initiation and consequently the crack formation, brittle material components are considered, and the redistribution of the thermal stresses during the high-speed crack formation is neglected.

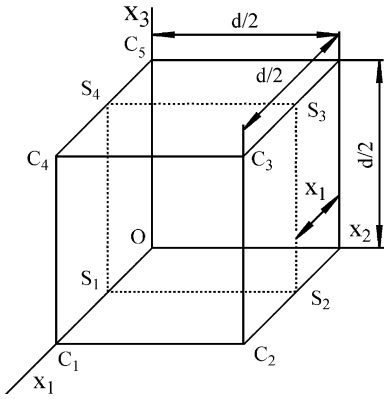

Fig. 5 The surface $S_1S_2S_3S_4 \perp x_1$ in the position $x_1 \in \langle 0, d/2 \rangle$ in one eighth of the cubic cell (see Figs. 3, 4)

Derived formulae for the critical particle radii resulting in the crack initiation in a particle and in a matrix, and the critical particle volume fraction resulting in maximal resistance against mechanical loading enable to predict and design properties of composite materials with adequate accuracy, as additionally confirmed by a good agreement of calculated values of investigated parameters for the SiC–Si_3N_4 multi-particle-matrix system with those from experimental results [11, 16].

Additionally, with regard to theoretical physicists, derived formulae for the x_1-dependent gradient W_s, representing an energy barrier with the maximal value W_{smax}, both presented in the section 'Theoretical background', can be incorporated to physicist-created analytical models describing the interaction of the thermal-stress induced energy barrier with dislocations or magnetic domain walls.

Theoretical background

Isotropic multi-particle-matrix system

Thermal stresses

The thermal radial and tangential stresses, σ_r and σ_φ, σ_v, derived in the system of the spherical coordinates

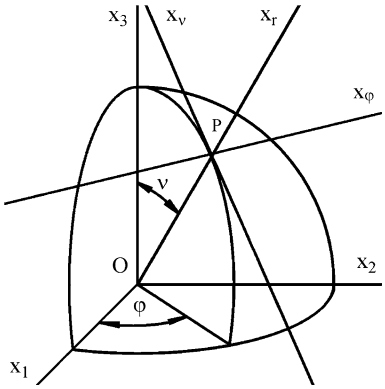

Fig. 6 The axes x_r, x_φ, x_v, and the point P with the position determined by the coordinates $(r = |OP|, \varphi, v)$, where O is the spherical particle centre. The radial and tangential stresses in the particle ($q = p$) and in the matrix ($q = m$), σ_{rq} and $\sigma_{\varphi q}$, σ_{vq}, act in the point P along the axes x_r and x_φ, x_v, respectively

(r, φ, v) related to the Cartesian system $(Ox_1x_2x_3)$ (see Fig. 6), are investigated in the point P of a continuum along the axes x_r and x_φ, x_v of the Cartesian system $(Px_rx_\varphi x_v)$, where r is the distance from the spherical particle centre O.

Resulting from the analytical model presented in [13], the radial and tangential stresses of the cubic cell, acting in the spherical particle (q = p) for $r \in \langle 0, R\rangle$ and in the cubic matrix ($q = m$) for $r \in \langle R, r_c\rangle$ (see Eq. 4), σ_{rq} and $\sigma_{\varphi q}$, σ_{vq}, respectively, have the forms

$$\sigma_{rp} = \sigma_{\varphi p} = \sigma_{vp} = -p_b, \tag{11}$$

$$\sigma_{rm} = -p_b\left\{1 + c_6\left[1 - \left(\frac{R}{r}\right)^3\right]\right\}, \tag{12}$$

$$\sigma_{\varphi m} = \sigma_{vm} = -p_b\left\{1 + c_6\left[1 + \frac{1}{2}\left(\frac{R}{r}\right)^3\right]\right\}, \tag{13}$$

where $\sigma > 0$ and $\sigma < 0$ represent the tensile and compressive stresses, respectively.

The compressive or tensile particle-matrix boundary radial stress, $p_b > 0$ or $p_b < 0$, respectively, is derived as [13]

$$p_b = c_7 \int_T^{T_i} (\alpha_m - \alpha_p)\, \mathrm{d}T, \tag{14}$$

where the coefficient c_i ($i = 1 - 10$) is presented in the section Appendix (see Eqs. 116–125); T_i and T are the initial and final temperatures of a cooling process, respectively; α_q is the thermal expansion coefficient of the particle ($q = p$) and the matrix ($q = m$). Considering α_q to be temperature-independent, the integral $\int_T^{T_i} \alpha_q\, \mathrm{d}T$ is replaced by $\alpha_q(T_i - T)$.

Temperature range of cooling process

With regard to a real composite material as the precipitate-matrix system, the initial temperature $T_i \leq (0.35 - 0.5)_m$ represents the relaxation temperature of the multi-particle-matrix system below which the stress relaxation does not occur as a consequence of thermal-activated processes [11, 16], where T_m is the minimum of the set $\{T_{mp}, T_{mm}\}$, and T_{mp}, T_{mm} are melting points of the precipitate (= particle), the matrix, respectively.

The thermal stresses exhibit an maximal value on the particle-matrix boundary, acted by the radial stress, p_b (see Eq. 14). Accordingly, the presented derivations are considered in the temperature range $T \in \langle T_c, T_i\rangle$, where T_c is the critical final temperature of a cooling process at which the stress, $|p_b| = \sigma_{yq}$, where $\sigma_{yq} = \sigma_{ycq}$ or $\sigma_{yq} = \sigma_{ytq}$ is a yield stress in compression or tension related to the compressive or tensile stress, $p_b > 0$ or $p_b < 0$, respectively, and if $\sigma_{yp} < \sigma_{ym}$ or $\sigma_{yp} > \sigma_{ym}$ then $\sigma_{yq} = \sigma_{yp}$ or $\sigma_{yq} = \sigma_{ym}$, respectively. With regard to Eq. 14, the critical temperature, T_c, can be derived from

$$\left|c_7 \int_{T_c}^{T_i} (\alpha_m - \alpha_p)\, \mathrm{d}T\right| - \sigma_{yq} = 0, \tag{15}$$

for a real isotropic multi-particle-matrix system by a numerical method, and considering α_q ($q = p,m$) to be temperature-independent, T_c has the form

$$T_c = T_i - \frac{\sigma_{yq}}{|c_7(\alpha_m - \alpha_p)|}. \tag{16}$$

If the particle-matrix boundary bond is characterized by the adhesion radial stress, p_a, and loaded by the tensile radial stress, $p_b < 0$, the presented derivations are considered for $|p_b| \leq p_a$, the critical temperature, T_a, related to the condition, $|p_b| = p_a$, can be derived from Eq. 15, or has the form given by Eq. 16, both for $\sigma_{yq} \to p_a$. If $T_a > T_c$, the presented derivations are considered in the temperature range $T \in \langle T_a, T_i\rangle$.

Finally, with regard to plastic-deformable and ceramic multi-particle-matrix systems, a contribution to thermal stresses at temperature $T < T_c$ is released by plastic deformation and the system cracking [11, 16], respectively.

Elastic energy density

Applying the Hooke laws for an isotropic continuum [1]

$$\varepsilon_{11} = s_{11}\sigma_{11} + s_{12}(\sigma_{22} + \sigma_{33}), \tag{17}$$

$$\varepsilon_{22} = s_{11}\sigma_{22} + s_{12}(\sigma_{11} + \sigma_{33}), \tag{18}$$

$$\varepsilon_{33} = s_{11}\sigma_{33} + s_{12}(\sigma_{11} + \sigma_{22}), \tag{19}$$

into the formula for the elastic energy density [1]

$$w = \frac{1}{2}\sum_{i,j=1-3}^{3} \varepsilon_{ij}\sigma_{ij}, \tag{20}$$

and with regard to ε_{ij}, $\sigma_{ij} = 0$ ($i \neq j$) and the subscript transformations, $11 \rightarrow r$, $22 \rightarrow \varphi$, $33 \rightarrow v$, the elastic energy density of the thermal stresses in the spherical particle and in the cubic cell matrix, w_p and w_m, respectively, are derived as

$$w_p = \frac{3p_b^2}{2}\left(s_{11p} + 2s_{12p}\right), \tag{21}$$

$$w_m = \frac{3p_b^2}{4}\left[2c_8^2(s_{11m} + 2s_{12m}) + c_6^2(s_{11m} - s_{12m})\left(\frac{R}{r}\right)^6\right]. \tag{22}$$

where the elastic moduli, s_{11q}, s_{12q} [1], for the particle ($q = p$) and the matrix ($q = m$) are presented in the section Appendix (see Eqs. 114, 115).

Curve integral of elastic energy density

The curve integrals within the cubic cell, W_{cp}, W_{cm1} and W_{cm2}, as integrals of w_p, w_m and w_m (see Eqs. 21, 22) along the abscissae P_1P_2, P_2P_3 and P_4P_5 in the plane x_1x_3 in the positions $x_1 \in \langle 0, R\rangle$ and $x_1 \in \langle R, d/(2\cos\varphi)\rangle$ (see Fig. 7), respectively, as the elastic energy 'curve' density, equivalent to those along the abscissae in the planes x_1x_2, x_2x_3 due to the isotropy of the multi-particle-matrix system, are derived as

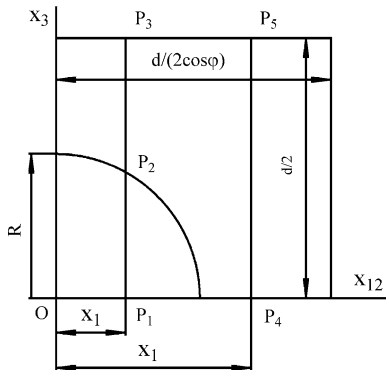

Fig. 7 The abscissae $P_1P_2P_3$ and P_4P_5 in the plane $x_{12}x_3$ (see Fig. 4) in the positions $x_1 \in \langle 0, R\rangle$ and $x_1 \in \langle 0, d/(2\cos\varphi)\rangle$, respectively, perpendicular to the axis x_{12}, where $x_{12} \subset x_1x_2$ and $\varphi = \sphericalangle(x_{12}, x_1) \in \langle 0, \pi/4\rangle$

$$W_{cp} = \int_{P_1P_2} w_p\,\mathrm{d}x_3 = \frac{3p_b^2}{2}\left(s_{11p} + 2s_{12p}\right)\sqrt{R^2 - x_1^2}, \quad x_1 \in \langle 0, R\rangle, \tag{23}$$

$$W_{cm1} = \int_{P_2P_3} w_m\,\mathrm{d}x_3 = \frac{3p_b^2}{20}\left(5c_8^2(s_{11m}+2s_{12m})\left[R\left(\frac{4\pi}{3v}\right)^{1/3} - 2\sqrt{R^2-x_1^2}\right] + c_6^2R(s_{11m}-s_{12m}) \times\left\{1-\left[\frac{2R(3v)^{1/3}}{\sqrt{R^2(4\pi)^{2/3}+4x_1^2(3v)^{2/3}}}\right]^5\right\}\right), \quad x_1 \in \langle 0, R\rangle, \tag{24}$$

$$W_{cm2} = \int_{P_4P_5} w_m\,\mathrm{d}x_3 = \frac{3p_b^2R}{20}\left(5c_8^2(s_{11m}+2s_{12m})\left(\frac{4\pi}{3v}\right)^{1/3} + c_6^2(s_{11m}-s_{12m})\left(\frac{R}{x_1}\right)^5 \times\left\{1-\left[\frac{2x_1(3v)^{1/3}}{\sqrt{R^2(4\pi)^{2/3}+4x_1^2(3v)^{2/3}}}\right]^5\right\}\right), \quad x_1 \in \left\langle R, \frac{d}{2}\right\rangle, \tag{25}$$

where $\varphi = \angle(x_1x_{12}) \in \langle 0, 2\pi\rangle$ and the axis $x_{12} \subset x_1x_2$ (see Fig. 4); $|P_1P_2| = \sqrt{R^2 - x_1^2}$; $|P_2P_3| = d/2 - \sqrt{R^2 - x_1^2}$ and $|P_4P_5| = d/2$ for $x_1 \in \langle 0, R\rangle$ and $x_1 \in \langle R, d/2\rangle$, respectively. With regard to the term r^{-6} in Eq. 22, and due to the isotropy of the multi-particle-matrix system, the elastic energy accumulated in the cubic cell matrix between the points P_2 and P_3, and between the points P_4 and P_5, is equal to that accumulated between the points at radii $r = |OP_2| = R$ and $r = |OP_3| = \sqrt{(d/2)^2 + x_1^2}$, and at the radii $r = |OP_4| = x_1$ and $r = |OP_5| = \sqrt{(d/2)^2 + x_1^2}$, for $x_1 \in \langle 0, R\rangle$ and $x_1 \in \langle R, d/2\rangle$, respectively. Accordingly, the term $r^{-6}\,\mathrm{d}x_3$ (see Eqs. 22–24) is replaced by $r^{-6}\,\mathrm{d}r$, where $r \in \langle R, |OP_3|\rangle$ and $r \in \langle x_1, |OP_5|\rangle$ for $x_1 \in \langle 0, R\rangle$ and $x_1 \in \langle R, d/2\rangle$, respectively.

Particle and matrix crack initiation and formation

Provided that $p_b < 0$ and then for $\alpha_m < \alpha_p$, or $p_b > 0$ and then for $\alpha_m > \alpha_p$ (see Eqs. 11–14), the spherical particle or the cubic cell matrix are acted by the tensile

thermal stresses, or the tensile radial thermal stress and the compressive tangential thermal stresses, respectively, and consequently, as a consequence of releasing of the elastic energy of the thermal stresses, equal circular cracks are assumed to be equivalently created in the planes x_1x_2, x_1x_3, x_2x_3 in the spherical particle or the cell matrix (see Fig. 6), due to the isotropy of the multi-particle-matrix system. Resulting from the isotropy of the multi-particle-matrix system, the formulae (23)–(25) are also related to the plane $x_1'x_3$, and accordingly the particle or matrix cracks, symmetrical with respect to the formation plane x_1x_2 (see Figs. 8–13), exhibit the same shape in all planes $x_{12}x_3$, where the axis $x_{12} \subset x_1x_2$ and $\varphi = \angle(x_1x_{12}) \in \langle 0, 2\pi \rangle$ (see Fig. 4).

The curve integrals, W_{cp} and W_{cm1} (see Eqs. 23, 24), represent decreasing and increasing functions of $x_1 \in \langle 0, R \rangle$, respectively, both depending on the parameter R, where $(W_{cp})_{x_1=R} = 0$, and accordingly the sum, $W_{cp} + W_{cm1}$, is a decreasing, increasing or decreasing–

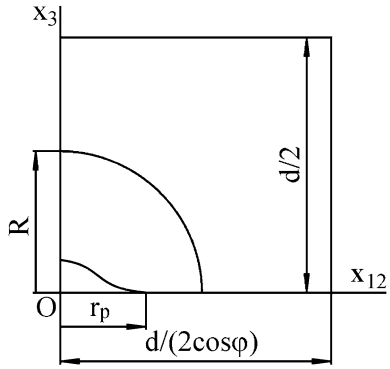

Fig. 8 The particle crack initialized and consequently formed in the plane $x_{12}x_3$ (see Fig. 4) for $R > R_{p1}$ from the particle centre, O, to the particle surface; the particle crack radius, r_p, for $R \in \langle R_{p1}, R_{p2} \rangle$

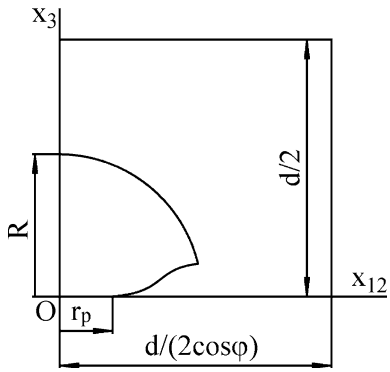

Fig. 9 The particle crack initialized and consequently formed in the plane $x_{12}x_3$ (see Fig. 4) for $R > R_{p2}$ from the particle surface to the particle centre, O; the particle crack radius, r_p, for $R \in \langle R_{p2}, R_{p1} \rangle$

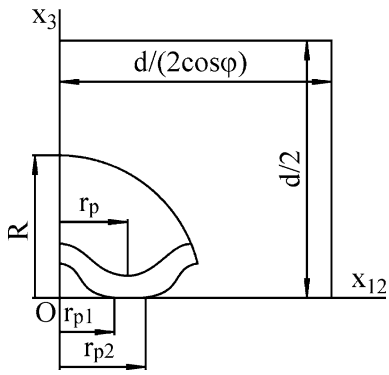

Fig. 10 The particle crack simultaneously initialized and formed in the plane $x_{12}x_3$ (see Fig. 4) for $R > R_{p1} = R_{p2}$ from the particle centre, O, to the particle surface, and vice versa; the particle crack radii, r_{p1} and r_{p2}, of the disconnected cracks for $R \in \langle R_{p1}, R_{p1/2} \rangle$; the position, r_p, of the minimum of the interconnected cracks for $R \geq R_{p1/2}$

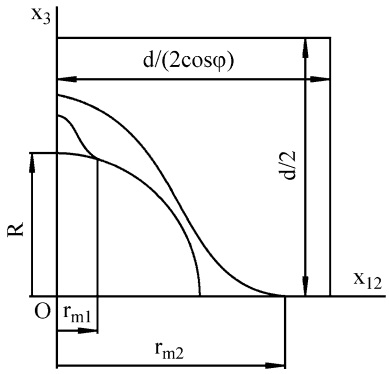

Fig. 11 The matrix cracks initialized and formed in the plane $x_{12}x_3$ (see Fig. 4) from the position $x_1 = 0$ to the position $x_1 \in \langle 0, r_{m1} \rangle$, $x_1 \in \langle 0, R \rangle$ and from the position $x_1 = R$ to the position $x_1 \in \langle R, r_{m2} \rangle$, $x_1 \in \langle R, d/(2\cos\varphi) \rangle$ for $R \in \langle R_{m1}, R_{m2} \rangle$, $R \geq R_{m2}$ and $R \in \langle R_{m2}, R_{m3} \rangle$, $R \geq R_{m3}$, respectively; the matrix crack radii, r_{m1}, r_{m2}

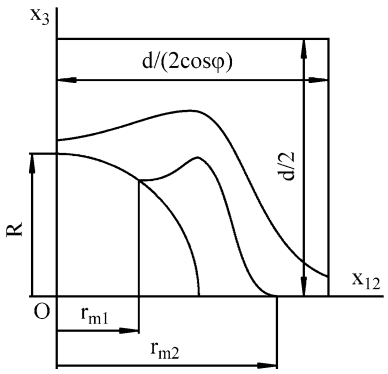

Fig. 12 The matrix cracks initialized and formed in the plane $x_{12}x_3$ (see Fig. 4) from the position $x_1 = R$ to the positions $x_1 \in \langle r_{m1}, R \rangle$, $x_1 \in \langle 0, R \rangle$ and $x_1 \in \langle R, r_{m2} \rangle$, $x_1 \in \langle R, d/(2\cos\varphi) \rangle$ for $R \in \langle R_{m2}, R_{m1} \rangle$, $R \geq R_{m1}$ and $R \in \langle R_{m2}, R_{m3} \rangle$, $R \geq R_{m3}$, respectively; the matrix crack radii, r_{m1}, r_{m2}

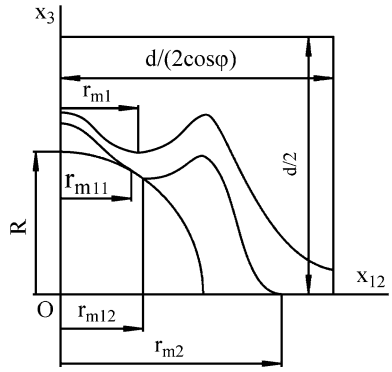

Fig. 13 The matrix cracks simultaneously initialized and formed in the plane $x_{12}x_3$ (see Fig. 4) from the positions $x_1 = 0$ and $x_1 = R$ to the positions $x_1 \in \langle 0, r_{m11}\rangle$, $x_1 \in \langle 0, r_{m1}\rangle$ and $x_1 \in \langle r_{m12}, R\rangle$, $x_1 \in \langle r_{m1}, R\rangle$ for $R \in \langle R_{m1}, R_{m1/2}\rangle$, $R \geq R_{m1/2}$, respectively, and from the position $x_1 = R$ to the position $x_1 \in \langle R, r_{m2}\rangle$, $x_1 \in \langle R, d/(2\cos\varphi)\rangle$ for $R \in \langle R_{m2}, R_{m3}\rangle$, $R \geq R_{m3}$, respectively; the matrix crack radii, r_{m11}, r_{m12}, of the disconnected cracks; the position, r_{m1}, of the minimum of the interconnected cracks

increasing dependence on $x_1 \in \langle 0, R\rangle$, exhibiting a minimum as a function of the parameter R. With regard to the decreasing, increasing or decreasing–increasing x_1-dependence of the sum, the circular particle crack is thus formed from the particle centre, O, to the particle surface (see Fig. 8), vice versa (see Fig. 9), or simultaneously from the particle centre and the particle surface (see Fig. 10), resulting from the conditions, $(W_{cp} + W_{cm1})_{x_1=0} > (W_{cm1})_{x_1=R}$, $(W_{cp} + W_{cm1})_{x_1=0} < (W_{cm1})_{x_1=R}$ or $(W_{cp} + W_{cm1})_{x_1=0} = (W_{cm1})_{x_1=R}$, from which the coefficient, c_9 (see Eq. 124), is determined as $c_9 > 0$, $c_9 < 0$ or $c_9 = 0$, and consequently, the function, f_p, represents a decreasing, increasing or decreasing-increasing x_1-dependence, respectively.

Similarly, with regard to $c_9 > 0$, $c_9 < 0$ or $c_9 = 0$, the matrix crack is formed from the position $x_1 = 0$ to the position $x_1 = R$ (see Fig. 11), vice versa (see Fig. 12), or simultaneously from the positions $x_1 = 0$ and $x_1 = R$ (see Fig. 13), respectively.

Considering $c_9 > 0$, $c_9 < 0$ and $c_9 = 0$, critical particle radii, as reasons of the formation of particle and matrix cracks of the infinitesimal length, are determined with respect to positions of the maximum value of $W_{cp} + W_{cm1}$, then for $x_1 = 0$, $x_1 = R$ and $x_1 = 0$ or $x_1 = R$, respectively.

The coefficient c_9 depends on the particle volume fraction, v, and on the material parameters of the particle, s_{11p}, s_{12p}, and considering c_9 as a function of v, the critical particle volume fraction, $v_0 \in (0, \pi/6)$, related to determination of a direction of the particle cracking, can be derived from the condition, $c_9 = 0$, for a concrete isotropic multi-particle-matrix system by a numerical method.

Particle crack initiation and formation I After the particle crack formation, the elastic energy, $\mathrm{d}W_p = (W_{cp} + W_{cm1})x_1\,\mathrm{d}\varphi\,\mathrm{d}x_1/3$, accumulated in the cubic cell infinitesimal volume of the dimensions $x_1\,\mathrm{d}\varphi \times \mathrm{d}x_1 \times d/2$, and being a consequence of the particle cracking of the infinitesimal surface area, $\mathrm{d}S_p = x_1\,\mathrm{d}\varphi\,\mathrm{d}s_p$, is in the equilibrium state with the energy of an infinitesimal crack surface of the particle, $\mathrm{d}W_{csp} = \gamma_p\,\mathrm{d}s_p\,\mathrm{d}x_1\,\mathrm{d}\varphi$, and then $\mathrm{d}W_p = \mathrm{d}W_{csp}$ [11, 16], where the multiplication factor 1/3 results from the formation of equal circular particle cracks in the planes x_1x_2, x_1x_3, x_2x_3 (see Fig. 6); $\gamma_p = s_{11p}K_{ICp}^2$ [11, 16] is the particle crack surface energy per unit surface area; K_{ICp} is the particle fracture toughness; $\mathrm{d}s_p = \mathrm{d}x_1\sqrt{1 + (\partial f_p/_1)^2}$ [17] is infinitesimal length of the curve, f_p, describing the particle crack shape in the interval $x_1 \in \langle 0, R\rangle$ (see Figs. 8–10), representing a function of x_1 and the parameter R, corresponding to the x_1- and R-dependence of $W_{cp} + W_{cm1}$. With regard to $\mathrm{d}W_p = \mathrm{d}W_{csp}$, we get

$$\frac{\partial f_p}{\partial x_1} = \pm\frac{1}{3s_{11p}K_{ICp}^2}\sqrt{(W_{cp} + W_{cm1})^2 - (3s_{11p}K_{ICp}^2)^2}, \tag{26}$$

and accordingly, the energy condition for the particle crack formation, is derived as

$$W_{cp} + W_{cm1} - 3s_{11p}K_{ICp}^2 > 0, \tag{27}$$

fulfilled for the particle radius greater than critical, as a reason of the particle cracking.

Considering such v when $c_9 > 0$ (see Eq. 124), the critical particle radii, R_{p1} and R_{p2}, as a reason of the crack initiation and consequently the crack formation in the particle from the particle centre, O, to the particle surface, and as a reason of the particle crack tip on the particle surface (see Fig. 8), represent roots of Eqs. 28 and 29 in the forms

$$(W_{cp} + W_{cm1})_{x_1=0} - 3s_{11p}K_{ICp}^2 = 0, \tag{28}$$

$$(W_{cp} + W_{cm1})_{x_1=R} - 3s_{11p}K_{ICp}^2 = 0, \tag{29}$$

as functions of the variable R, resulting from the condition for the particle crack tip in the particle centre in the position $x_1 = 0$ and on the particle surface in the position $x_1 = R$, $(\partial f_p/\partial x_1)_{x_1=0} = 0$ and $(\partial f_p/\partial x_1)_{x_1=R} = 0$, respectively, related to an ideal-brittle particle [11, 16], where $R_{p1} < R_{p2}$ for

$c_9 > 0$. With regard to Eqs. 23, 24, 28, 29, R_{p1} and R_{p2} are derived as

$$\frac{1}{R_{p1}} = \frac{1}{2s_{11p}}\left(\frac{p_b}{K_{ICp}}\right)^2 \times \left(s_{11p} + 2s_{12p} + \frac{1}{10}\left\{5c_8^2(s_{11m} + 2s_{12m})\left[\left(\frac{4\pi}{3\nu}\right)^{1/3} - 2\right] + c_6^2(s_{11m} - s_{12m})\left[1 - 32\left(\frac{3\nu}{4\pi}\right)^{5/3}\right]\right\}\right), \tag{30}$$

$$\frac{1}{R_{p2}} = \frac{1}{20s_{11p}}\left(\frac{p_b}{K_{ICp}}\right)^2 \times \left(5c_8^2(s_{11m} + 2s_{12m})\left(\frac{4\pi}{3\nu}\right)^{1/3} + c_6^2(s_{11m} - s_{12m})\left\{1 - \left[\frac{2(3\nu)^{1/3}}{\sqrt{(4\pi)^{2/3} + 4(3\nu)^{2/3}}}\right]^5\right\}\right). \tag{31}$$

The particle crack radius (see Fig. 8), r_p, determining the particle crack tip position, representing a root of the equation

$$W_{cp} + W_{cm1} - 3s_{11p}K_{ICp}^2 = 0, \tag{32}$$

as a function of the variable x_1 and the parameter $R \in \langle R_{p1}, R_{p2}\rangle$, resulting from the condition for the particle crack tip in the position $x_1 = r_p$, $\left(\partial f_p/\partial x_1\right)_{x_1 = r_p} = 0$ (see Eq. 26), can be derived from Eq. 32 for a concrete isotropic multi-particle-matrix system by a numerical method, where $r_p = 0$ and $r_p = R_{p2}$ for $R = R_{p1}$ and $R = R_{p2}$, respectively.

With regard to Eq. 26, the function, f_p, describing the particle crack shape in the intervals $x_1 \in \langle 0, r_p\rangle$ and $x_1 \in \langle 0, R\rangle$ for $R \in \langle R_{p1}, R_{p2}\rangle$ and $R \geq R_{p2}$ (see Fig. 8), respectively, has the form

$$f_p = \frac{1}{3s_{11p}K_{ICp}^2} \times \left[\beta_p - \int \sqrt{\left(W_{cp} + W_{cm1}\right)^2 - \left(3s_{11p}K_{ICp}^2\right)^2}\,\mathrm{d}x_1\right], \tag{33}$$

representing a decreasing function of x_1, and accordingly the sign – in Eq. 26 is considered. The integral can be derived for a concrete isotropic multi-particle-matrix system by a numerical method, and with respect to the boundary conditions given by Eqs. 34 and 35 in the forms

$$x_1 = r_p, \quad f_p = 0, \tag{34}$$

$$R = R_{p2}, \quad x_1 = R_{p2}, \quad f_p = 0, \tag{35}$$

related to the particle radius $R \in \langle R_{p1}, R_{p2}\rangle$ and $R \geq R_{p2}$, respectively, the integration constant, β_p, is derived for $R \in \langle R_{p1}, R_{p2}\rangle$ as

$$\beta_p = \left[\int \sqrt{\left(W_{cp} + W_{cm1}\right)^2 - \left(3s_{11p}K_{ICp}^2\right)^2}\,\mathrm{d}x_1\right]_{x_1 = r_p}, \tag{36}$$

and for $R \geq R_{p2}$ as

$$\beta_p = \left[\int \sqrt{\left(W_{cp} + W_{cm1}\right)^2 - \left(3s_{11p}K_{ICp}^2\right)^2}\,\mathrm{d}x_1\right]_{x_1 = R_{p2};\, R = R_{p2}}. \tag{37}$$

Particle crack initiation and formation II Considering such ν when $c_9 < 0$ (see Eq. 124), the critical particle radii, R_{p2} and R_{p1} (see Eqs. 30, 31), are a reason of the crack initiation and consequently the crack formation in the particle from the particle surface in the position $x_1 = R$ to the particle centre, O, and a reason of the particle crack tip in the particle centre in the position $x_1 = 0$ (see Fig. 9), respectively, where $R_{p2} < R_{p1}$ for $c_9 < 0$.

With regard to Eq. 26, the function, f_p, describing the particle crack shape in the intervals $x_1 \in \langle r_p, R\rangle$ and $x_1 \in \langle 0, R\rangle$ for $R \in \langle R_{p2}, R_{p1}\rangle$ and $R \geq R_{p1}$ (see Fig. 9), respectively, has the form

$$f_p = \frac{1}{3s_{11p}K_{ICp}^2} \times \left[\beta_p + \int \sqrt{\left(W_{cp} + W_{cm1}\right)^2 - \left(3s_{11p}K_{ICp}^2\right)^2}\,\mathrm{d}x_1\right], \tag{38}$$

representing an increasing function of x_1, and accordingly the sign + in Eq. 26 is considered. With respect to the boundary conditions given by Eqs. 39 and 40 in the forms

$$x_1 = r_p, \quad f_p = 0, \tag{39}$$

$$R = R_{p1}, \quad x_1 = 0, \quad f_p = 0, \tag{40}$$

related to the particle radius $R \in \langle R_{p2}, R_{p1}\rangle$ and $R \geq R_{p1}$, respectively, the integration constant, β_p, is derived for $R \in \langle R_{p2}, R_{p1}\rangle$ as

$$\beta_p = -\left[\int \sqrt{\left(W_{cp}+W_{cm1}\right)^2-\left(3s_{11p}K_{ICp}^2\right)^2}\,\mathrm{d}x_1\right]_{x_1=r_p}, \tag{41}$$

and for $R \geq R_{p1}$ as

$$\beta_p = -\left[\int \sqrt{\left(W_{cp}+W_{cm1}\right)^2-\left(3s_{11p}K_{ICp}^2\right)^2}\,\mathrm{d}x_1\right]_{x_1=0;\,R=R_{p1}}. \tag{42}$$

The particle crack radius (see Fig. 9), r_p (see Eq. 41), represents a root of Eq. 32, as a function of the variable x_1 and the parameter $R \in \langle R_{p2}, R_{p1}\rangle$, and can be derived from Eq. 32, along with the integral in Eq. 38, for a concrete isotropic multi-particle-matrix system by a numerical method, where $r_p = 0$ and $r_p = R_{p1}$ for $R = R_{p2}$ and $R = R_{p1}$, respectively.

Particle crack initiation and formation III Considering such v when $c_9 = 0$ (see Eq. 124), the critical particle radii, R_{p1}, R_{p2} and $R_{p1/2}$, are a reason of the crack initiation and consequently the crack formation in the particle simultaneously from the particle centre in the position $x_1 = 0$ and from the particle surface in the position $x_1 = R$, and a reason of the particle crack tip in the position $x_1 = R/2$ (see Fig. 10), respectively, where $R_{p1} = R_{p2}$ for $c_9 = 0$, and $R_{p1/2} > R_{p1}$ represents a root of Eq. 28 as a function of the variable R on the condition $x_1 = R/2$ in the form

$$\frac{1}{R_{p1/2}} = \frac{1}{20s_{11p}}\left(\frac{p_b}{K_{ICp}}\right)^2 \times \left(5c_8^2(s_{11m}+2s_{12m})\left[\left(\frac{4\pi}{3v}\right)^{1/3}-\sqrt{3}\right] + c_6^2(s_{11m}-s_{12m})\left\{1-\left[\frac{2(3v)^{1/3}}{\sqrt{(4\pi)^{2/3}+(3v)^{2/3}}}\right]^5\right\}\right). \tag{43}$$

The particle crack is described by the functions, f_{p1} and f_{p2}, decreasing and increasing in the intervals $x_1 \in \langle 0, r_{p1}\rangle$, $x_1 \in \langle 0, r_p\rangle$ and $x_1 \in \langle r_{p2}, R\rangle$, $x_1 \in \langle r_p, R\rangle$ (see Fig. 10), respectively, related to the disconnected, interconnected particle cracks, as depended on the parameter R. The particle crack radii, r_{p1}, r_{p2}, and the position in which the function, $f_p = f_{p1} + f_{p2}$, describing the interconnected particle cracks exhibits a minimum, r_p, represent roots of Eq. 32, as a function of the variable x_1 and the parameter R, for $R \in \langle R_{p1}, R_{p1/2}\rangle$ and $R_{p1/2}$, respectively, and can be derived from Eq. 32 for a concrete isotropic multi-particle-matrix system by a numerical method, where $r_{p1} = r_{p2} = 0$ and $r_{p1} = r_{p2} = R_{p1/2}/2$ for $R = R_{p1}$ and $R = R_{p1/2}$, respectively.

With respect to the boundary conditions given by Eqs. 44– 46 in the forms

$$x_1 = r_{p1}, \quad f_{p1} = 0, \tag{44}$$

$$x_1 = r_{p2}, \quad f_{p2} = 0, \tag{45}$$

$$R = R_{p1/2}, \quad x_1 = \frac{R_{p1/2}}{2}, \quad f_{p1} = f_{p2} = 0, \tag{46}$$

related to the particle radius $R \in \langle R_{p1}, R_{p1/2}\rangle$ and $R \geq R_{p1/2}$, respectively, the functions, f_{p1} and f_{p2}, are given by Eqs. 33, 36, 37, and Eqs. 38, 41, 42, on the conditions $x_1 = r_{p1}$ and $x_1 = r_{p2}$ in Eqs. 36 and 41 for $R \in \langle R_{p1}, R_{p1/2}\rangle$, respectively, and on the condition $x_1 = R_{p1/2}$, $R = R_{p1/2}$ in Eqs. 37, 42 for $R_{p1/2}$.

Matrix crack initiation and formation I Considering the particle-matrix boundary adhesion radial stress, p_a, provided that $p_b > 0$ and then for $\alpha_m < \alpha_p$, the c_a-multiple of σ_{rm}, $\sigma_{\varphi m}$, $\sigma_{\nu m}$, and c_a^2 -multiple of w_p, w_m, the latter resulted from the dependence, $w \propto \sigma^2$ (see Eq. 20), are concerned in the matrix crack formation, where the multiplier, c_a, is derived as

$$c_a = 1 - \frac{p_a}{p_b}. \tag{47}$$

After the matrix crack initialization and formation, the elastic energy related to the positions $x_1 \in \langle 0, R\rangle$ and $x_1 \in \langle 0, d/2\rangle$, $\mathrm{d}W_m = c_a^2\left(W_{cp}+W_{cm1}\right)x_1\,\mathrm{d}\varphi\,\mathrm{d}x_1/3$ and $\mathrm{d}W_m = c_a^2 W_{cm2}x_1\,\mathrm{d}\varphi\,\mathrm{d}x_1/3$, respectively, accumulated in the cubic cell infinitesimal volume of the dimensions $x_1\,\mathrm{d}\varphi \times \mathrm{d}x_1 \times d/2$, and being a consequence of the matrix cracking of the infinitesimal surface area, $\mathrm{d}S_m = x_1\,\mathrm{d}\varphi\,\mathrm{d}s_m$, is in the equilibrium state with the energy of an infinitesimal crack surface of the matrix, $\mathrm{d}W_{csmi} = \gamma_m \mathrm{d}s_{mi}\,\mathrm{d}x_1\,\mathrm{d}\varphi$ $(i = 1,2)$, and then $\mathrm{d}W_m = \mathrm{d}W_{csmi}$ [11, 16], where the multiplication factor 1/3 results from the formation of equal circular particle cracks in the planes x_1x_2, x_1x_3, x_2x_3 (see Fig. 6); $\gamma_m = s_{11m}K_{ICm}^2$, where the multiplication factor 1/3 results from the is the matrix crack surface energy per unit surface area; K_{ICm} is the matrix fracture toughness; $\mathrm{d}s_{mi} = \mathrm{d}x_1\sqrt{1+\left(_{mi}/\partial x_1\right)^2}$ [17] is infinites-

imal length of the curves, f_{m1} and f_{m2}, describing the matrix crack shape in the intervals $x_1 \in \langle 0, R\rangle$ and $x_1 \in \langle R, d/(2\cos\varphi)\rangle$ (see Fig. 11), respectively, representing functions of x_1 and the parameter R, corresponding to the x_1- and R-dependence of W_{cm2}, where $\varphi = \angle(x_1 x_{12}) \in \langle 0, 2\pi\rangle$ and the axis $x_{12} \subset x_1 x_2$ (see Fig. 4). With regard to $\mathrm{d}W_m = \mathrm{d}W_{csmi}$, we get

$$\frac{\partial f_{m1}}{\partial x_1} = \pm\frac{1}{3s_{11m}K_{ICm}^2}\sqrt{c_a^4\left(W_{cp}+W_{cm1}\right)^2-\left(3s_{11m}K_{ICm}^2\right)^2}, \tag{48}$$

$$\frac{\partial f_{m2}}{\partial x_1} = -\frac{1}{3s_{11m}K_{ICm}^2}\sqrt{c_a^4 W_{cm2}^2-\left(3s_{11m}K_{ICm}^2\right)^2}, \tag{49}$$

and accordingly, the energy condition for the particle crack formation, is derived in the interval $x_1 \in \langle 0, R\rangle$ as

$$c_a^2\left(W_{cp}+W_{cm1}\right)-3s_{11m}K_{ICm}^2>0, \tag{50}$$

and in the interval $x_1 \in \langle R, d/(2\cos\varphi)\rangle$ as

$$c_a^2 W_{cm2}-3s_{11m}K_{ICm}^2>0, \tag{51}$$

both fulfilled for the particle radius greater than critical, as a reason of the matrix cracking.

Considering such ν when $c_9>0$ (see Eq. 124), the critical particle radii, R_{m1} and R_{m2}, as a reason of the crack initiation and consequently the crack formation in the matrix from the position $x_1 = 0$ to the position $x_1>0$, and as a reason of the matrix crack tip in the position $x_1 = R$ (see Fig. 11), represent roots of Eqs. 52 and 53 in the forms

$$c_a^2\left(W_{cp}+W_{cm1}\right)_{x_1=0}-3s_{11m}K_{ICm}^2 = 0, \tag{52}$$

$$c_a^2\left(W_{cm2}\right)_{x_1=R}-3s_{11m}K_{ICm}^2 = 0, \tag{53}$$

as functions of the variable R, resulting from the conditions for the matrix crack tip, $\left(\partial f_{m1}/_1\right)_{x_1=0}= 0$ and $\left(\partial f_{m1}/_1\right)_{x_1=R}= 0$, respectively, related to an ideal-brittle particle [11, 16], where $R_{m1}<R_{m2}$ for $c_9>0$. With regard to Eqs. 35, 36, 52, 53, R_{m1} and R_{m2} are derived as

$$\frac{1}{R_{m1}}=\frac{1}{2s_{11m}}\left(\frac{c_a p_b}{K_{ICm}}\right)^2 \times\left(s_{11p}+2s_{12p}+\frac{1}{10}\left\{5c_8^2(s_{11m}+2s_{12m})\left[\left(\frac{4\pi}{3\nu}\right)^{1/3}-2\right] +c_6^2(s_{11m}-s_{12m})\left[1-32\left(\frac{3\nu}{4\pi}\right)^{5/3}\right]\right\}\right). \tag{54}$$

$$\frac{1}{R_{m2}}=\frac{1}{20s_{11m}}\left(\frac{c_a p_b}{K_{ICm}}\right)^2 \times\left(5c_8^2(s_{11m}+2s_{12m})\left(\frac{4\pi}{3\nu}\right)^{1/3} +c_6^2(s_{11m}-s_{12m})\left\{1-\left[\frac{2(3\nu)^{1/3}}{\sqrt{(4\pi)^{2/3}+4(3\nu)^{2/3}}}\right]^5\right\}\right). \tag{55}$$

The matrix crack radius (see Fig. 11), r_{m1}, determining the matrix crack tip position, representing a root of the equation

$$c_a^2\left(W_{cp}+W_{cm1}\right)-3s_{11m}K_{ICm}^2 = 0, \tag{56}$$

as a function of the variable x_1 and the parameter $R \in \langle R_{m1}, R_{m2}\rangle$, resulting from the condition for the particle crack tip in the position $x_1 = r_{m1}$, $\left(\partial f_{m1}/\partial x_1\right)_{x_1=r_{m1}} = 0$ (see Eq. 48), can be derived from Eq. 56 for a concrete isotropic multi-particle-matrix system by a numerical method, where $r_{m1} = 0$ and $r_{m1} = R_{m2}$ for $R = R_{m1}$ and $R = R_{m2}$, respectively.

With regard to Eq. 48, the function, f_m, describing the matrix crack shape in the intervals $x_1 \in \langle 0, r_{m1}\rangle$ and $x_1 \in \langle 0, R\rangle$ for $R \in \langle R_{m1}, R_{m2}\rangle$ and $R \geq R_{m2}$ (see Fig. 11), respectively, has the form

$$f_{m1} = \frac{1}{3s_{11m}K_{ICm}^2} \times\left[\beta_{m1}-\int\sqrt{c_a^4\left(W_{cp}+W_{cm1}\right)^2-\left(3s_{11m}K_{ICm}^2\right)^2}\,\mathrm{d}x_1\right], \tag{57}$$

representing a decreasing function of x_1, and accordingly the sign - in Eq. 48 is considered. The integral can be derived for a concrete isotropic multi-particle-matrix system by a numerical method, and with respect to the boundary conditions given by Eqs. 58 and 59 in the forms

$$x_1 = r_{m1}, \quad f_{m1} = \sqrt{R^2-r_{m1}^2}, \tag{58}$$

$$x_1 = R, \quad \left(f_{m1}\right)_{x_1=R}= \left(f_{m2}\right)_{x_1=R}, \tag{59}$$

related to the particle radius $R \in \langle R_{m1}, R_{m2}\rangle$ and

$R \geq R_{m2}$, respectively, the integration constant, β_{m1}, is derived for $R \in \langle R_{m1}, R_{m2}\rangle$ as

$$\beta_{m1} = 3s_{11m}K_{ICm}^2\sqrt{R^2 - r_{m1}^2} + \left[\int \sqrt{c_a^4\left(W_{cp} + W_{cm1}\right)^2 - \left(3s_{11m}K_{ICm}^2\right)^2}\,\mathrm{d}x_1\right]_{x_1=r_{m1}}, \tag{60}$$

and for $R \geq R_{m2}$ as

$$\beta_{m1} = \beta_{m2} - \left\{\int \left[\sqrt{c_a^4 W_{cm2}^2 - \left(3s_{11m}K_{ICm}^2\right)^2} - \sqrt{c_a^4\left(W_{cp} + W_{cm1}\right)^2 - \left(3s_{11m}K_{ICm}^2\right)^2}\right]\mathrm{d}x_1\right\}_{x_1=R}, \tag{61}$$

where the function, f_{m2}, and the integration constant, β_{m2}, are given by Eqs. 76 and 79, 80, respectively.

Matrix crack initiation and formation II Considering such v when $c_9 < 0$ (see Eq. 124), the critical particle radii, R_{m2} and R_{m1}, are a reason of the crack initiation and consequently the crack formation in the matrix from the position $x_1 = R$ to the position $x_1 < R$, and a reason of the matrix crack tip in the position $x_1 = 0$ (see Fig. 12), respectively, where $R_{m2} < R_{m1}$ for $c_9 < 0$.

With regard to Eq. 48, the function, f_{m1}, describing the matrix crack shape in the intervals $x_1 \in \langle 0, r_{m1}\rangle$ and $x_1 \in \langle 0, R\rangle$ for $R \in (R_{m2}, R_{m1})$ and $R \geq R_{m1}$ (see Fig. 12), respectively, has the form

$$f_{m1} = \frac{1}{3s_{11m}K_{ICm}^2} \times \left[\beta_{m1} + \int \sqrt{c_a^4\left(W_{cp} + W_{cm1}\right)^2 - \left(3s_{11m}K_{ICm}^2\right)^2}\,\mathrm{d}x_1\right], \tag{62}$$

representing an increasing function of x_1, and accordingly the sign + in Eq. 48 is considered. With respect to the boundary conditions given by Eqs. 58 and 59 related to the particle radius $R \in \langle R_{m2}, R_{m1}\rangle$ and R_{m1}, respectively, the integration constant, β_{m1}, is derived for $R \in \langle R_{m2}, R_{m1}\rangle$ as

$$\beta_{m1} = 3s_{11m}K_{ICm}^2\sqrt{R^2 - r_{m1}^2} - \left[\int \sqrt{c_a^4\left(W_{cp} + W_{cm1}\right)^2 - \left(3s_{11m}K_{ICm}^2\right)^2}\,\mathrm{d}x_1\right]_{x_1=r_{m1}}, \tag{63}$$

and for $R \geq R_{m1}$ as

$$\beta_{m1} = \beta_{m2} - \left\{\int \left[\sqrt{c_a^4 W_{cm2}^2 - \left(3s_{11m}K_{ICm}^2\right)^2} + \sqrt{c_a^4\left(W_{cp} + W_{cm1}\right)^2 - \left(3s_{11m}K_{ICm}^2\right)^2}\right]\mathrm{d}x_1\right\}_{x_1=R}, \tag{64}$$

where the function, f_{m2}, and the integration constant, β_{m2}, are given by Eqs. 76 and 79, 80, respectively. The matrix crack radius (see Fig. 12), r_{m1} (see Eq. 63), represents a root of Eq. 56, as a function of the variable x_1 and the parameter $R \in \langle R_{m2}, R_{m1}\rangle$, and can be derived from Eq. 56, along with the integral in Eq. 62, for a concrete isotropic multi-particle-matrix system by a numerical method, where $r_{m1} = 0$ and $r_{m1} = R_{m1}$ for $R = R_{m2}$ and $R = R_{m1}$, respectively.

Matrix crack initiation and formation III Considering such v when $c_9 = 0$ (see Eq. 124), the critical particle radii, R_{m1}, R_{m2} and $R_{m1/2}$, are a reason of the crack initiation and consequently the crack formation in the matrix simultaneously from the positions $x_1 = 0$, $x_1 = R$ to the positions $x_1 > 0$, $x_1 < R$, respectively, and a reason of the matrix crack tip in the position $x_1 = R/2$ (see Fig. 13), respectively, where $r_{m1} = R_{m2}$ for $c_9 = 0$, and $R_{m1/2 > R_{m1}}$ represents a root of Eq. 52 as a function of the variable R on the condition $x_1 = R/2$ in the form

$$\frac{1}{R_{m1/2}} = \frac{1}{4s_{11m}}\left(\frac{c_a p_b}{K_{ICm}}\right)^2 \times \left(\sqrt{3}\left(s_{11p} + 2s_{12p}\right) + c_8^2\left(s_{11m} + 2s_{12m}\right)\left[\left(\frac{4\pi}{3v}\right)^{1/3} - \sqrt{3}\right] + \frac{c_6^2}{5}\left(s_{11m} - s_{12m}\right)\left\{1 - \left[\frac{2(3v)^{1/3}}{\sqrt{(4\pi)^{2/3} + (3v)^{2/3}}}\right]^5\right\}\right). \tag{65}$$

The matrix crack is described by the functions, f_{m11} and f_{m12}, decreasing and increasing in the intervals $x_1 \in \langle 0, r_{m11}\rangle$, $x_1 \in \langle 0, r_{m1}\rangle$ and $x_1 \in \langle r_{m12}, R\rangle$, $x_1 \in \langle r_{m1}, R\rangle$ (see Fig. 13), respectively, related to the disconnected, interconnected matrix cracks, as depended on the parameter R. The matrix crack radii, r_{m11}, r_{m12}, and the position in which the function, $f_{m1} = f_{m11} + f_{m12}$, describing the interconnected particle cracks exhibits a minimum, r_{m1}, represent roots of Eq. 56, as a function of the variable x_1 and the

parameter R, for $R \in \langle R_{m1}, R_{m1/2} \rangle$ and $R \geq R_{m1/2}$, respectively, and can be derived from Eq. 56 for a concrete isotropic multi-particle-matrix system by a numerical method, where $r_{m11} = r_{m12} = 0$ and $r_{m11} = r_{m12} = R_{m1/2}/2$ for $R = R_{m1}$ and $R = R_{m1/2}$, respectively.

With regard to Eq. 48, the functions, f_{m11} and f_{m12}, have the forms

$$f_{m11} = \frac{1}{3s_{11m}K_{ICm}^2} \times \left[\beta_{m11} - \int \sqrt{c_a^4\left(W_{cp} + W_{cm1}\right)^2 - \left(3s_{11m}K_{ICm}^2\right)^2}\,\mathrm{d}x_1\right], \tag{66}$$

$$f_{m12} = \frac{1}{3s_{11m}K_{ICm}^2} \times \left[\beta_{m12} + \int \sqrt{c_a^4\left(W_{cp} + W_{cm1}\right)^2 - \left(3s_{11m}K_{ICm}^2\right)^2}\,\mathrm{d}x_1\right], \tag{67}$$

representing increasing and decreasing function of x_1, and accordingly the sign – and + in Eqs. 66 and 70 are considered, respectively. The integrals can be derived for a concrete isotropic multi-particle-matrix system by a numerical method, and with respect to the boundary conditions given by Eqs. 68, 69 and 70, 74 in the forms

$$x_1 = r_{m11}, \quad f_{m11} = \sqrt{R^2 - r_{m11}^2}, \tag{68}$$

$$x_1 = r_{m12}, \quad f_{m12} = \sqrt{R^2 - r_{m12}^2}, \tag{69}$$

$$x_1 = r_{m1}, \quad f_{m11} = f_{m12}, \tag{70}$$

$$x_1 = r_{m1}, \quad f_{m11} = f_{m12}, \tag{71}$$

related to the particle radius $R \in \langle R_{m1}, R_{m1/2} \rangle$ and $R \geq R_{m1/2}$, respectively, the integration constants, β_{m11} and β_{m12}, are given by Eqs. 45 and 54, replacing the term r_{m1} by the terms r_{m11} and r_{m12}, respectively, for $R \in \langle R_{m1}, R_{m1/2} \rangle$, and derived for $R \geq R_{m1/2}$ as

$$\begin{aligned}\beta_{11m} &= \beta_{m2} + 2\left[\int \sqrt{c_a^4\left(W_{cp}+W_{cm1}\right)^2 - \left(3s_{11m}K_{ICm}^2\right)^2}\,\mathrm{d}x_1\right]_{x_1=r_{m1}} \\ &\quad - \left[\int \sqrt{c_a^4\left(W_{cp}+W_{cm1}\right)^2 - \left(3s_{11m}K_{ICm}^2\right)^2}\,\mathrm{d}x_1\right]_{x_1=R} \\ &\quad - \left[\int \sqrt{c_a^4 W_{cm2}^2 - \left(3s_{11m}K_{ICm}^2\right)^2}\,\mathrm{d}x_1\right]_{x_1=R},\end{aligned} \tag{72}$$

$$\begin{aligned}\beta_{m12} &= \beta_{m2} - \left[\int \sqrt{c_a^4\left(W_{cp} + W_{cm1}\right)^2 - \left(3s_{11m}K_{ICm}^2\right)^2}\,\mathrm{d}x_1\right]_{x_1=R} \\ &\quad - \left[\int \sqrt{c_a^4 W_{cm2}^2 - \left(3s_{11m}K_{ICm}^2\right)^2}\,\mathrm{d}x_1\right]_{x_1=R},\end{aligned} \tag{73}$$

where the function, f_{m2}, and the integration constant, β_{m2}, are given by Eqs. 76, 79, 80, respectively.

Matrix crack initiation and formation IV With regard to the function, f_{m2}, describing the matrix crack shape in the interval $x_1 \in \langle R, d/(2\cos\varphi) \rangle$ (see Figs. 4, 12, 13), the critical particle radius, R_{m2}, given by Eq. 55, is also a reason of the crack initiation and consequently the crack formation in the matrix from the position $x_1 = R$ to the position $x_1 > R$. Consequently, the critical particle radius, R_{m3}, resulting from the condition for the matrix crack tip on the cell surface in the position $x_1 = d/(2\cos\varphi)$, $(m2/\partial x_1)_{x_1 = d/(2\cos\varphi)} = 0$, related to an ideal-brittle matrix [11, 16], corresponding to a connection of the matrix cracks in neighbouring cells between the points C_1 and C_{12} (see Fig. 4), where $R_{m2} < R_{m3}$, represents a root of Eq. 53 as a function of the variable R on the condition $x_1 = d/(2\cos\varphi)$, and regarding Eq. 3 is derived as an increasing function of the angle ϕ in the form

$$\begin{aligned}\frac{1}{R_{m3}} &= \frac{1}{20s_{11m}}\left(\frac{c_a p_b}{K_{ICm}}\right)^2 \\ &\quad \times \left\{5c_8^2(s_{11m} + 2s_{12m})\left(\frac{4\pi}{3v}\right)^{1/3}\right. \\ &\quad + 32c_6^2\cos^5\varphi(s_{11m} - s_{12m})\left(\frac{3v}{4\pi}\right)^{5/3} \\ &\quad \left.\times\left[1 - \frac{1}{(1+\cos^2\varphi)^{5/2}}\right]\right\}.\end{aligned} \tag{74}$$

The matrix crack radius (see Figs. 12, 13), r_{m2}, determining the matrix crack tip position, representing a root of the equation

$$c_a^2 W_{cm2} - 3s_{11m}K_{ICm}^2 = 0, \tag{75}$$

as a function of the variable x_1 and the parameter $R \in \langle R_{m2}, R_{m3} \rangle$, resulting from the condition for the particle crack tip in the position $x_1 = r_{m2}$, $(\partial f_{m2}/\partial x_1)_{x_1 = r_{m2}} = 0$ (see Eq. 49), can be derived from Eq. 75 for a concrete isotropic multi-particle-matrix system by a numerical method.

With regard to Eq. 49, the function, f_{m2}, describing the matrix crack shape in the intervals $x_1 \in \langle R, r_{m2}\rangle$ and $x_1 \in \langle R, d/(2\cos\varphi)\rangle$ for $R \in \langle R_{m2}, R_{m3}\rangle$ and $R \geq R_{m3}$ (see Figs. 12, 13), respectively, has the form

$$f_{m2} = \frac{1}{3s_{11m}K_{ICm}^2} \times \left[\beta_{m2} - \int \sqrt{c_a^4 W_{cm2}^2 - \left(3s_{11m}K_{ICm}^2\right)^2}\,\mathrm{d}x_1\right]. \tag{76}$$

The integral can be derived for a concrete isotropic multi-particle-matrix system by a numerical method, and with respect to the boundary conditions given by Eqs. 77 and 78 in the forms

$$x_1 = r_{m2}, \quad f_{m2} = 0, \tag{77}$$

$$R = R_{m3}, \quad x_1 = \frac{d}{2\cos\varphi}, \quad f_{m2} = 0, \tag{78}$$

related to the particle radius $R \in \langle R_{m2}, R_{m3}\rangle$ and $R \geq R_{m3}$, respectively, the integration constant, β_{m1}, is derived for $R \in \langle R_{m2}, R_{m3}\rangle$ as

$$\beta_{m2} = \left[\int \sqrt{c_a^4 W_{cm2}^2 - \left(3s_{11m}K_{ICm}^2\right)^2}\,\mathrm{d}x_1\right]_{x_1 = r_{m2}}, \tag{79}$$

and for $R \geq R_{m3}$ as

$$\beta_{m2} = \left[\int \sqrt{c_a^4 W_{cm2}^2 - \left(3s_{11m}K_{ICm}^2\right)^2}\,\mathrm{d}x_1\right]_{x_1 = d/(2\cos\varphi);\, R = R_{m3}}. \tag{80}$$

Surface integral of elastic energy density

The surface integral, W_{sp} and W_{sm1}, of w_p and w_m (see Eqs. 21, 22) over the surfaces $P_2P_3P_4 \parallel x_2x_3$ and $P_1P_2P_4P_5 \parallel x_2x_3$ (Fig. 14), representing the elastic energy gradient within the spherical particle and the cubic cell matrix along the axis $x_1 \in \langle 0, R\rangle$ (Figs. 3, 14), $W_{sp} = \partial W_p/\partial x_1$ and $W_{sm1} = \partial W_m/\partial x_1$, respectively, as the elastic energy 'surface' density, equivalent to those along the axes x_2, x_3 due to the isotropy of the multi-particle-matrix system, has the form

$$W_{sp} = \int_{S_p} w_p\,\mathrm{d}S_p = 4\int_0^{\pi/2}\int_0^{R_2} w_p r_{23}\,\mathrm{d}r_{23}\,\mathrm{d}\xi = \frac{3\pi p_b^2}{2}\left(s_{11p} + 2s_{12p}\right)\left(R^2 - x_1^2\right), 1 \in \langle 0, R\rangle, \tag{81}$$

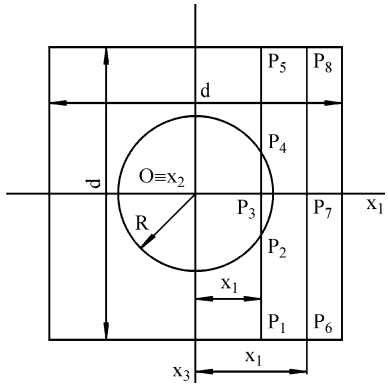

Fig. 14 The planes $P_1P_2P_3P_4P_5 \parallel x_2x_3$ and $P_6P_7P_8 \parallel x_2x_3$ in the positions $x_1 \in \langle 0, R\rangle$ and $x_1 \in \langle R, d/2\rangle$, respectively, in the cubic cell of the dimension d, containing the spherical particle of the radius R (Fig. 3)

$$W_{sm1} = \int_{S_m} w_m\,\mathrm{d}S_m = 8\int_0^{\pi/4}\int_{R_2}^{R_{23}} w_m r_{23}\,\mathrm{d}r_{23}\,\mathrm{d}\xi = \frac{3p_b^2}{8}\left\{4c_8^2(s_{11m} + 2s_{12m})\left[R^2\left(\frac{4\pi}{3v}\right)^{2/3} - \pi\left(R^2 - x_1^2\right)\right] + R^2c_6^2(s_{11m} - s_{12m})\left(\pi - 4c_{11}R^4\right)\right\}, \quad x_1 \in \langle 0, R\rangle, \tag{82}$$

and then, for $x_1 \in \langle 0, R\rangle$, $\mathrm{d}S_q = r_{23}\,\mathrm{d}r_{23}\,\mathrm{d}\xi$ is an infinitesimal part in the point P of the spherical particle (q = p) or the cubic cell matrix (q = m) on the surfaces $S_p \equiv P_2P_{31}P_{32} \parallel x_2x_3$ or $S_m \equiv P_{11}P_2P_{32}P_{33}P_{12} \parallel x_2x_3$ for $r_{23} \in \langle 0, R_2\rangle$ or $r_{23} \in \langle R_2, R_{23}\rangle$ (Figs. 14, 15), respectively, where $P_2P_{31}P_{32}, P_{11}P_2P_{32}P_{33}P_{12} \subset P_1P_2P_3P_4P_5$ (Fig. 14); $r_{23} = |P_{31}P|$; $P_{31}P_2x_3$; $R = |OP_2| = |OP_{32}|$;

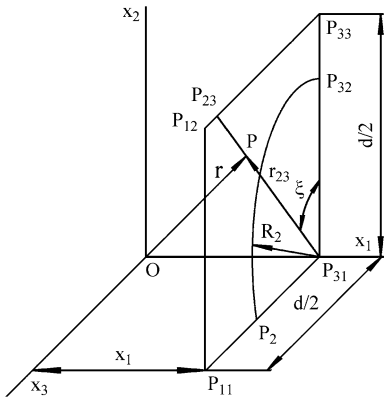

Fig. 15 The planes $P_2P_{31}P_{32} \parallel x_2x_3$ and $P_{11}P_2P_{32}P_{33}P_{23}P_{12} \parallel x_2x_3$ of the spherical particle of the radius R and of the cubic cell matrix of the dimension d (Fig. 3), included, along with the point P, in the plane $P_1P_2P_3P_4P_5 \parallel x_2x_3$ in the position $x_1 \in \langle 0, R\rangle$ (Fig. 14)

$R_2 = |P_{31}P_2| = |P_{31}P_{32}| = \sqrt{R^2 - x_1^2}$;
$R_{23} = |P_{31}P_{23}| = d/(2\cos\xi)$; $P_{31}P_2, P_{31}P_{23} \parallel x_2x_3$; and the coordinate r in Eq. 22 is derived as $r = |OP| = \sqrt{r_{23}^2 + x_1^2}$. Due to the isotropy of the multi-particle-matrix system, the angle ξ is sufficient to be varied in the interval $\xi \in \langle 0, \pi/4\rangle$.

The surface integral, W_{sm2}, of w_m (see Eq. 22) over the surface $P_6P_7P_8 \parallel x_2x_3$ (Fig. 14), representing the elastic energy gradient within the cubic cell along the axis $x_1 \in \langle R, d/2\rangle$ (Figs. 3, 14), $W_{sm2} = \partial W_m/\partial x_1$, equivalent to those along the axes x_2, x_3, has the form

$$W_{sm2} = \int_{S_m} w_m \,\mathrm{d}S_m = 8\int_0^{\pi/4}\int_0^{R_{67}} w_m r_{67}\,\mathrm{d}r_{67}\,\mathrm{d}\xi$$
$$= \frac{3p_b^2R^2}{8}\left\{4c_8^2\left(\frac{4\pi}{3\nu}\right)^{2/3}(s_{11m}+2s_{12m}) + c_6^2(s_{11m}-s_{12m})\left(\pi - 4c_{11}x_1^4\right)\left(\frac{R}{x_1}\right)^4\right\},$$
$$x_1 \in \left\langle R, \frac{d}{2}\right\rangle, \tag{83}$$

and then, for $x_1 \in \langle R, d/2\rangle$, $\mathrm{d}S_m = r_{67}\,\mathrm{d}r_{67}\,\mathrm{d}\xi$ is an infinitesimal part in the point P of the cubic cell matrix on the surface $S_m 62P_{72}P_{73}P_{63} \parallel x_2x_3$ (Figs. 14, 16) for $r_{67} = |P_{71}P| \in \langle 0, R_{67}\rangle$, respectively, where $P_{61}P_{71}P_{72}P_{67}P_{62}6P_7P_8$ (Fig. 14); $P_{71}P \parallel x_2x_3$; $R_{67} = |P_{71}P_{67}| = d/(2\cos\xi)$; $P_{71}P_{67} \parallel x_2x_3$; and the coordinate r in Eq. 22 is derived as $r = |OP| = \sqrt{r_{67}^2 + x_1^2}$. Due to the isotropy of the multi-particle-matrix system, the angle ξ is sufficient to be varied in the interval $\xi \in \langle 0, \pi/4\rangle$.

Alternatively, the surface integral, W_{sm2}, of w_m (see Eq. 22) over the surface $P_6P_7P_8 \parallel x_2x_3$ (Fig. 14), is also derived as

$$W_{sm2} = \int_{S_m} w_m \,\mathrm{d}S_m = 4\int_0^{\varphi_{73}}\int_{\nu_6}^{\pi/2} w_m r^2\,\mathrm{d}\varphi\,\mathrm{d}\nu$$
$$= \frac{3p_b^2R^2}{8}\left[4c_8^2\left(\frac{4\pi}{3\nu}\right)^{2/3}(s_{11m}+2s_{12m}) + c_6^2c_{17}(s_{11m}-s_{12m})\left(\frac{R}{x_1}\right)^4\right],$$
$$x_1 \in \left\langle R, \frac{d}{2}\right\rangle, \tag{84}$$

and then, for $x_1 \in \langle R, d/2\rangle$, $\mathrm{d}S_m = r^2\,\mathrm{d}\varphi\,\mathrm{d}\nu$ represents an infinitesimal part in the point P of the cubic cell matrix on the surface $S_m 62P_{72}P_{73}P_{63} \parallel x_2x_3$ (Figs. 14, 17) for $r = |OP| = x_1/(\cos\varphi\sin\nu)$, $\varphi \in \langle 0, \varphi_{73}\rangle$, $\nu \in \langle \nu_6, \pi/2\rangle$, where $P_{62}P_{72}P_{73}P_{63} \subset P_6P_7P_8$ (Fig. 14); and the angles $\varphi_{73} = \angle(OP_{72}, OP_{73})$, $\nu_6 = \angle(x_3, OP_6)$ are presented in the section Appendix (see Eqs. 134, 135).

The x_1-dependence of $W_{sp} + W_{sm1}$ and W_{sm2} exhibits concave and convex courses in the intervals $x_1 \in \langle 0, R\rangle$ and $x_1 \in \langle R, d/2\rangle$, respectively. As a reason of material properties (e.g. coercivity, dislocation motion) [11], the maximum, $W_{\mathrm{smax}} = (W_{sp} + W_{sm1})_{x_1=0}$ (see Eqs. 81, 82), has the form

$$W_{\mathrm{smax}} = \frac{3\pi p_b^2R^2}{2}(s_{11p}+2s_{12p}) + \frac{3p_b^2R^2}{8}\left\{4c_8^2(s_{11m}+2s_{12m})\left[\left(\frac{4\pi}{3\nu}\right)^{2/3} - \pi\right] + c_6^2(s_{11m}-s_{12m})\left(\pi - 4c_{11}R^4\right)\right\}. \tag{85}$$

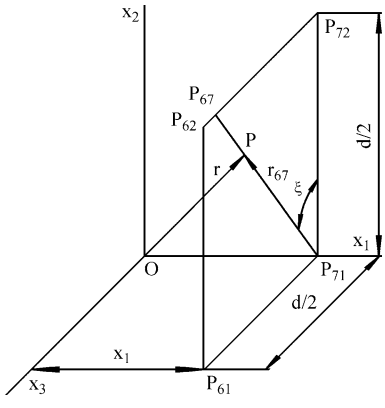

Fig. 16 The plane $P_{62}P_{72}P_{73}P_{68}P_{63} \parallel x_2x_3$ of the cubic cell matrix of the dimension d (Fig.3), included, along with the point P, in the plane $P_6P_7P_8 \parallel x_2x_3$ in the position $x_1 \in \langle R, d/2\rangle$ (Fig.14)

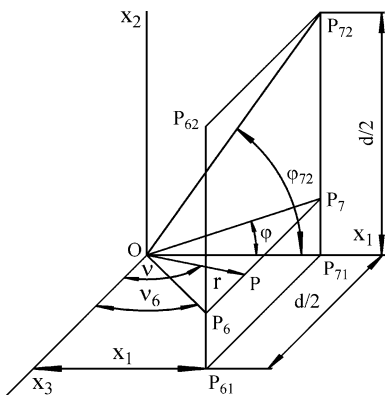

Fig. 17 The plane $P_{62}P_{72}P_{73}P_{63} \parallel x_2x_3$ of the cubic cell matrix of the dimension d (Fig. 3), included, along with the point P, in the plane $P_6P_7P_8 \parallel x_2x_3$ in the position $x_1 \in \langle R, d/2\rangle$ (Fig. 14)

Particle and matrix thermal-stress induced strengthening

Considering the planes $P_1P_2P_3P_4P_5$ and $P_6P_7P_8$ to be loaded by the stress, σ, constant over the individual plane in the positions $x_1\langle 0,R\rangle$ and $x_1\langle R,d/2\rangle$, respectively, the elastic energy density, $w_{\sigma q}$, induced by the stress, σ_q, acting along the axis x_1 in the particle ($q = p$) and the cubic cell matrix ($q = m$), is derived as [1]

$$w_{\sigma_q} = \frac{\varepsilon_{11q}\sigma_q}{2} = \frac{s_{11q}\sigma_q^2}{2}. \tag{86}$$

where ε_{11q} is the strain along the axis x_1.

The elastic energy gradient within the spherical particle and the cubic cell along the axis x_1 (Figs. 3, 14) is $W_{s\sigma_q} = \int_{S_q} w_{\sigma_q} S_q$, where $S_p \equiv P_2P_3P_4$, $S_m \equiv P_1P_2P_4P_5$ and $S_m \equiv P_6P_7P_8$ for $x_1\langle 0,R\rangle$ and $x_1\langle R,d/2\rangle$, respectively. The stresses, σ_p and σ_{mi}, derived from the conditions, $W_{s\sigma_p} = W_{sp}$ and $W_{s\sigma_{mi}} = W_{smi}$ (i = 1,2) (see Eqs. 81–84), and accordingly inducing the same influence as induced by the thermal stresses and thus representing the thermal-stress induced strengthening within the spherical particle and the cubic cell matrix, as a resistance against compressive and tensile mechanical loading for $\alpha_m > \alpha_p$ and $\alpha_m < \alpha_p$, respectively, have the forms

$$\sigma_p = p_b\sqrt{3\left(1+\frac{2s_{12p}}{s_{11p}}\right)}, \tag{87}$$

$$\sigma_{m1} = \pm\sqrt{\frac{W_{sm1}}{c_{18}}}, \tag{88}$$

$$\sigma_{m2} = \pm\sqrt{\frac{W_{sm2}}{c_{19}}}, \tag{89}$$

where Eqs. 88 and 89 are functions of $x_1 \in \langle 0,R\rangle$ (i = 1) and $x_1 \in \langle R,d/2\rangle$ (i = 2), respectively, and $(\sigma_{m1})_{x_1=R} = (\sigma_{m2})_{x_1=R}$ (see Eqs. 82–84, 136, 137). The signs + and – in Eqs. 88–90 are considered for $\alpha_m > \alpha_p$ and $\alpha_m < \alpha_p$, respectively.

With regard to the x_1-dependences, the parameters σ_{m1}, σ_{m2} are considered to represent matrix microstrengthening in the intervals $x_1 \in \langle 0,R\rangle$, $x_1 \in \langle R,d/2\rangle$ [11], respectively, and consequently the average value $\overline{\sigma}_m$, representing the thermal-stress induced strengthening in the cubic cell matrix, is defined, regarding Eq. 3, as [17]

$$\begin{aligned}\overline{\sigma}_m &= \frac{2}{d}\left(\int_0^R \sigma_{m1}\,\mathrm{d}x_1 + \int_R^{d/2}\sigma_{m2}\,\mathrm{d}x_1\right)\\ &= \pm\frac{2}{R}\left(\frac{3v}{4\pi}\right)^{1/3}\left(\int_0^R\sqrt{\frac{W_{sm1}}{c_{18}}}\mathrm{d}x_1 + \int_R^{d/2}\sqrt{\frac{W_{sm2}}{c_{19}}}\mathrm{d}x_1\right),\end{aligned} \tag{90}$$

where the integrals can be derived for a concrete isotropic particle-matrix system by a numerical method.

Isotropic one-particle-matrix system

As presented in the section 'Isotropic multi-particle-matrix system', concerning the v-dependences of thermal-stress related parameters of the SiC–Si_3N_4 multi-particle-matrix system in the interval $v \in \langle 0,\pi/6\rangle$, formulae related to the isotropic one-particle-matrix system represented by one spherical particle with the radius R embedded in the infinite matrix, as transformation of those related to the isotropic multi-particle-matrix system for $v = 0$, are required to be derived.

Thermal stresses

Resulting from the analytical model presented in [15], the radial and tangential stresses, acting in the spherical particle ($q = p$) for $r \in \langle 0,R\rangle$ and in the infinite matrix ($q = m$) for $r \in \langle R,\infty\rangle$, σ_{rq} and $\sigma_{\varphi q}$, σ_{vq}, respectively, have the forms

$$\sigma_{rp} = \sigma_{\varphi p} = \sigma_{vp} = -p_b, \tag{91}$$

$$\sigma_{rm} = -2\sigma_{\varphi m} = -2\sigma_{vm} = -p_b\left(\frac{R}{r}\right)^3, \tag{92}$$

where $\sigma > 0$ and $\sigma < 0$ represent the tensile and compressive stresses, respectively.

The compressive or tensile particle-matrix boundary radial stress, $p_b > 0$ or $p_b < 0$, respectively, is derived as [15]

$$p_b = \frac{1}{c_{10}}\int_T^{T_i}(\alpha_m - \alpha_p)\,\mathrm{d}T, \tag{93}$$

and Eqs. 11–14 are transformed for $v = 0$ to Eqs. 91–93 for $(p_c)_{v=0} = 0$. Considering α_q to be temperature-independent, the integral $\int_T^{T_i}\alpha_q\,\mathrm{d}T$ is replaced by $\alpha_q(T_i - T)$.

Temperature range of cooling process

With regard to the section 'Temperature range of cooling process', the presented derivations are considered in the temperature range $T \in \langle T_c, T_i \rangle$, and the critical final temperature of a cooling process, T_c, can be derived from

$$\left| \frac{1}{c_{10}} \int_{T_c}^{T_i} (\alpha_m - \alpha_p)\, \mathrm{d}T \right| - \sigma_{yq} = 0, \tag{94}$$

for a concrete isotropic multi-particle-matrix system by a numerical method, and considering α_q $(q = p,m)$ to be temperature-independent, T_c has the form

$$T_c = T_i - \sigma_{yq} \left| \frac{c_{10}}{(\alpha_m - \alpha_p)} \right|. \tag{95}$$

Elastic energy density

With regard to Eq. 20, and consequently to $\sigma_{ij} = 0$ $(i \neq j)$ and the subscript transformations, $11 \to r$, $22 \to \varphi$, $33 \to v$, the elastic energy density of the thermal stresses in the infinite matrix, w_m, is derived as

$$w_m = \frac{3p_b^2}{4} (s_{11m} - s_{12m}) \left(\frac{R}{r} \right)^6. \tag{96}$$

The elastic energy density of the thermal stresses in the spherical particle, w_p, is given by Eq. 21, considering the particle-matrix boundary radial stress, p_b, derived by Eqs. 93, 125.

Curve integral of elastic energy density

The curve integrals within the spherical cell of the radius $R_c \to \infty$, W_{cm1} and W_{cm2}, as integrals of w_m (see Eq. 96) along the abscissae P_4P_5 and P_7P_8 in the plane x_1x_3 in the positions $x_1 \in \langle 0, R \rangle$ and $x_1 \in \langle R, R_c \rangle$ (see Fig. 18), respectively, as the elastic energy 'curve' density, equivalent to those along the abscissae in the planes x_1x_2, x_2x_3 due to the isotropy of the multi-particle-matrix system, are derived as

$$\begin{aligned} W_{cm1} &= \int_{P_4P_5} w_m \, \mathrm{d}x_3 \\ &= \frac{3Rp_b^2}{20} (s_{11m} - s_{12m}) \left[1 - \left(\frac{R}{R_c} \right)^5 \right] \\ &\overset{R_c \to \infty}{=} \frac{3Rp_b^2}{20} (s_{11m} - s_{12m}), \end{aligned} \tag{97}$$

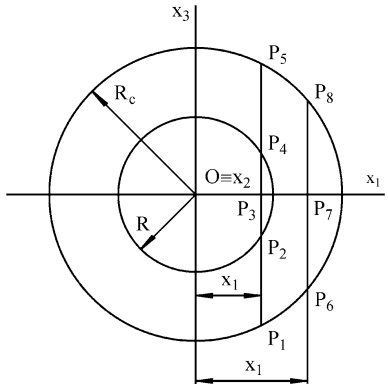

Fig. 18 The abscissae $P_1P_2P_3P_4P_5$ and $P_6P_7P_8$ in the positions $x_1 \in \langle 0, R \rangle$ and $x_1 \in \langle R, R_c \rangle$, respectively, in the spherical cell of the radius $R_c \to \infty$, containing the spherical particle of the radius R. With regard to surface integrals of w_p, w_m and w_m energy density (see section 'Surface integral of elastic energy density'), $P_1P_2P_3P_4P_5 \parallel x_2x_3$ and $P_6P_7P_8 \parallel x_2x_3$ represents planes, respectively

$$\begin{aligned} W_{cm2} &= \int_{P_7P_8} w_m \, \mathrm{d}x_3 \\ &= \frac{3Rp_b^2}{20} (s_{11m} - s_{12m}) \left(\frac{R}{x_1} \right)^5 \left[1 - \left(\frac{x_1}{R_c} \right)^5 \right] \\ &\overset{R_c \to \infty}{=} \frac{3Rp_b^2}{20} (s_{11m} - s_{12m}) \left(\frac{R}{x_1} \right)^5. \end{aligned} \tag{98}$$

With regard to the term r^{-6} in Eq. 96, and due to the isotropy of the one-particle-matrix system, the elastic energy accumulated in the cubic cell matrix between the points P_2 and P_3, and between the points P_4 and P_5, is equal to that accumulated between the points at radii $r = |OP_2| = R$ and $r = |OP_3| = R_c$, and at the radii $r = |OP_4| = x_1$ and $r = |OP_5| = R_c$, for $x_1 \in \langle 0, R \rangle$ and $x_1 \in \langle R, R_c \rangle$, respectively. Accordingly, the term $r^{-6}\,\mathrm{d}x_3$ (see Eqs. 96, 97, 98) is replaced by $r^{-6}\,\mathrm{d}r$, where $r \in \langle R, |OP_3| \rangle$ and $r \in \langle x_1, |OP_4| \rangle$ for $x_1 \in \langle 0, R \rangle$ and $x_1 \in \langle R, R_c \rangle$, respectively.

The curve integral within the spherical particle, W_{cp}, as an integral of w_p along the abscissae P_3P_4 in the plane x_1x_3 in the position $x_1 \in \langle 0, R \rangle$ (see Fig. 18), is given by Eq. 23, considering the particle-matrix boundary radial stress, p_b, derived by Eqs. 93, 125.

Particle and matrix crack initiation and formation

With regard to Eqs. 23, 97, $W_{cp} + W_{cm1}$ and W_{cm1} represent decreasing function of x_1, depending on the parameter R, and consequently the particle crack exhibits a shape as shown in Figs. 8, 11.

Particle crack initiation and formation The critical particle radii, R_{p1} and R_{p2}, where $R_{p2} > R_{p1}$, as a reason of the crack initiation and consequently the crack formation in the particle from the particle centre, O, in the position $x_1 = 0$, to the particle surface (see Fig. 8), and as a reason of the particle crack tip on the particle surface in the position $x_1 = R$, represent roots of Eqs. 28 and 29, respectively, in the forms

$$R_{p1} = \frac{20 s_{11p}}{10(s_{11p} + 2s_{12p}) + s_{11m} - s_{12m}} \left(\frac{K_{ICp}}{p_b}\right)^2, \tag{99}$$

$$R_{p2} = \frac{20 s_{11p}}{s_{11m} - s_{12m}} \left(\frac{K_{ICp}}{p_b}\right)^2. \tag{100}$$

The particle crack radius (see Fig. 8), r_p, determining the particle crack tip position, representing a root of Eq. 32, as a function of the variable x_1 and the parameter $R \in \langle R_{p1}, R_{p2}\rangle$, is derived as

$$r_p = \sqrt{R^2 - \frac{1}{(s_{11p}+2s_{12p})^2}\left[2 s_{11p}\left(\frac{K_{ICp}}{p_b}\right)^2 - \frac{R}{10}(s_{11m} - s_{12m})\right]^2}, \tag{101}$$

and the function, f_p, describing the particle crack shape in the intervals $x_1 \in \langle 0, r_p\rangle$ and $x_1 \in \langle 0, R\rangle$ for $R \in \langle R_{p1}, R_{p2}\rangle$ and $R \geq R_{p2}$ (see Fig. 8), is given by Eqs. 33, 36 and 37, respectively.

Matrix crack initiation and formation The critical particle radii, R_{m1} and R_{m2}, as a reason of the crack initiation and consequently the crack formation in the matrix from the position $x_1 = 0$ to the position $x_1 = R$, and as a reason of the matrix crack tip in the position $x_1 = R$ to the position $x_1 > R$ (see Fig. 21), represent roots of Eqs. 52 and 53, respectively, in the forms

$$R_{m1} = \frac{20 s_{11m}}{s_{11m} - s_{12m}} \left(\frac{K_{ICm}}{c_a p_b}\right)^2, \tag{102}$$

$$R_{m2} = \frac{20 s_{11m}}{10(s_{11p} + 2s_{12p}) + s_{11m} - s_{12m}} \left(\frac{K_{ICm}}{c_a p_b}\right)^2. \tag{103}$$

The matrix crack radii (see Fig.11), $r_{m1} \in \langle 0, R\rangle$ and $r_{m2} > R$, both for $R > R_m$, representing roots of Eqs. 56 and 75, as functions of the variable x_1 and the parameter R, for $R \in \langle R_{m1}, R_{m2}\rangle$ and $R \geq R_{m2}$, respectively, are derived as

$$r_{m1} = \sqrt{R^2 - \frac{1}{(s_{11p}+2s_{12p})^2}\left[2 s_{11m}\left(\frac{K_{ICm}}{c_a p_b}\right)^2 - \frac{R}{10}(s_{11m} - s_{12m})\right]^2}, \tag{104}$$

$$r_{m2} = \left[\frac{s_{11m} - s_{12m}}{20 s_{11m}}\left(\frac{c_a p_b R^3}{K_{ICm}}\right)^2\right]^{1/5}, \tag{105}$$

and the matrix crack (see Fig. 21) is thus described by Eqs. 57, 60, 61 and 76, 79 for $x_1 \in \langle 0, r_{m1}\rangle$ and $x_1 \in \langle R, r_{m2}\rangle$, related to $R \geq R_{m1}$ and R_{m2}, respectively.

Surface integral of elastic energy density

The surface integral, W_{sp}, of w_p (see Eq. 21) over the surface $P_2P_3P_4 \parallel x_2x_3$ (Fig. 18) is given by Eq. 81, considering the particle-matrix boundary radial stress, p_b, derived by Eq. 93. Determining the surface integral of the elastic energy density, the spherical particle is considered to be embedded in the spherical cell of the radius R_c (Fig. 18), and derived formulae then represent transformations of the integrals for $R_c \to \infty$.

The surface integral, W_{sm1}, of w_m (see Eqs. 93, 96) over the surface $P_1P_2P_4P_5 \parallel x_2x_3$ (Fig. 18), representing the elastic energy gradient within the spherical cell matrix of the radius $R_c \to \infty$ along the axis $x_1 \in \langle 0, R\rangle$, $W_{sm1} = \partial W_m/\partial x_1$, as the elastic energy 'surface' density, equivalent to that along the axes x_2, x_3 due to the isotropy of the one-particle-matrix system, has the form

$$\begin{aligned} W_{sm1} &= \int_{S_m} w_m \,\mathrm{d}S_m = 4\int_0^{\pi/2}\int_{R_2}^{R_1} w_m r_{23}\,\mathrm{d}r_{23}\,\mathrm{d}\xi \\ &= \frac{3\pi p_b^2 R^2}{8}(s_{11m} - s_{12m})\left[1 - \left(\frac{R}{R_c}\right)^4\right] \\ &\overset{R_c\to\infty}{=} \frac{3 p_b^2 R^2}{8}(s_{11m} - s_{12m}), \quad x_1 \in \langle 0, R\rangle, \end{aligned} \tag{106}$$

and then, for $x_1 \in \langle 0, R\rangle$, $\mathrm{d}S_q = r_{23}\,\mathrm{d}r_{23}\,\mathrm{d}\xi$ is an infinitesimal part in the point P of the spherical particle $(q = p)$ or the spherical cell matrix $(q = m)$ on the surfaces $S_p \equiv P_2P_{31}P_{32} \parallel x_2x_3$ or $S_m \equiv P_1P_2P_{32}P_{33} \parallel x_2x_3$, $P_2P_{31}P_{32}, P_1P_2P_{32}P_{33} \subset P_1P_2P_3P_4P_5$ (Fig. 18), for $r_{23} \in \langle 0, R_2\rangle$ or $r_{23} \in \langle R_2, R_1\rangle$ (Fig. 19), respectively, where $r_{23} = |P_{31}P|$, $P_{31}P \parallel x_2x_3$, $R = |OP_2| = |OP_{32}|$, $R_c = |OP_1| = |OP_{33}|$ (Fig. 15), $R_1 = |P_{31}P_1| = |P_{31}P_{33}| = \sqrt{R_c^2 - x_1^2}$, $R_2 = |P_{31}P_2| = |P_{31}P_{32}| = \sqrt{R_p^2 - x_1^2}$, $P_{31}P_1, P_{31}P_2 \parallel x_2x_3$;

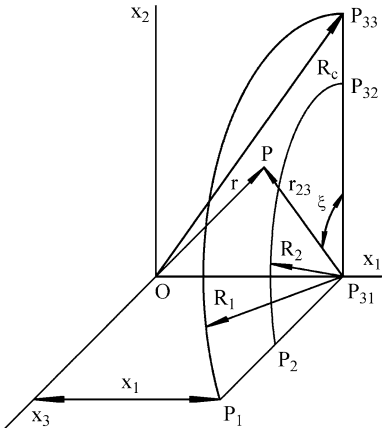

Fig. 19 The planes $P_2P_{31}P_{32} \parallel x_2x_3$ and $P_1P_2P_{32}P_{33}P_{23} \parallel x_2x_3$ of the spherical particle of the radius R and of the spherical cell matrix of the radius $R_c \to \infty$, included, along with the point P, in the plane $P_1P_2P_3P_4P_5 \parallel x_2x_3$ in the position $x_1 \in \langle 0, R\rangle$ (Fig. 18)

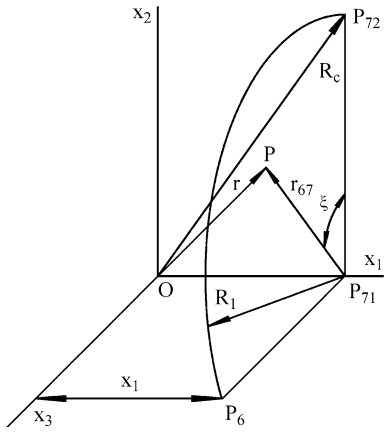

Fig. 20 The plane $P_6P_{72}P_{73} \parallel x_2x_3$ of the spherical cell matrix of the radius $R_c \to \infty$, included, along with the point P, in the plane $P_6P_7P_8 \parallel x_2x_3$ in the position $x_1 \in \langle R, R_c\rangle$ (Fig. 18)

and the coordinate r in Eq. 96 is derived as $r = |OP| = \sqrt{r_{23}^2 + x_1^2}$. Due to the isotropy of the particle-matrix system, the angle ξ is sufficient to be varied in the interval $\xi \in \langle 0, \pi/2\rangle$.

The surface integral, W_{sm2}, of w_m (see Eqs. 93, 96) over the surface $P_6P_7P_8 \parallel x_2x_3$ (Fig. 18), representing the elastic energy gradient within the spherical cell of the radius $R_c \to \infty$ along the axis $x_1 \in \langle R, R_c\rangle$ (Fig. 18), $W_{sm2} = \partial W_m/\partial x_1$, equivalent to those along the axes x_2, x_3, has the form

$$\begin{aligned} W_{sm2} &= \int_{S_m} w_{sm}\,\mathrm{d}S_m = 4\int_0^{\pi/2}\int_0^{R_{68}} w_m r_{68}\,\mathrm{d}r_{68}\,\mathrm{d}\xi \\ &= \frac{3R^2\pi p_b^2}{8}(s_{11m} - s_{12m})\left(\frac{R}{x_1}\right)^4\left[1 - \left(\frac{R}{R_c}\right)^4\right] \\ &\overset{R_c\to\infty}{=} \frac{3\pi p_b^2 R^2}{8}(s_{11m} - s_{12m})\left(\frac{R}{x_1}\right)^4, \\ &\quad x_1 \in \langle R, R_c\rangle, \quad R_c \to \infty, \end{aligned} \tag{107}$$

and then, for $x_1 \in \langle R, R_c\rangle$, $\mathrm{d}S_m = r_{68}\,\mathrm{d}r_{68}\,\mathrm{d}\xi$ is an infinitesimal part in the point P of the spherical cell matrix on the surface $S_m 62P_{72}P_{73}P_{63} \parallel x_2x_3$ (Fig. 20) for $r_{68} = |P_{72}P| \in \langle 0, R_{68}\rangle$, respectively, where $P_{62}P_{72}P_{73}P_{63} \subset P_6P_7P_8$ (Fig. 18); $P_{72}P \parallel x_2x_3$; $R_{68} = |P_{72}P_{68}| = \sqrt{R_c^2 - x_1^2}$; $P_{72}P_{68} \parallel x_2x_3$; and the coordinate r in Eq. 96 is derived as $r = |OP| = \sqrt{r_{68}^2 + x_1^2}$. Due to the isotropy of the particle-matrix system, the angle ξ is sufficient to be varied in the interval $\xi \in \langle 0, \pi/2\rangle$.

Consequently, the maximum, $W_{\mathrm{smax}} = (W_{sp} + W_{sm1})_{x_1=0}$, derived from Eqs. 81, 106 for $x_1 = 0$, has the form

$$W_{\mathrm{smax}} = \frac{3R^2\pi p_b^2}{8}\left[4(s_{11p} + 2s_{12p}) + s_{11m} - s_{12m}\right]. \tag{108}$$

Particle and matrix thermal-stress induced strengthening

The elastic energy gradients within the spherical cell matrix along the axis x_1, $W_{s\sigma_{m1}}$ and $W_{s\sigma_{m2}}$, equivalent to those along the axes x_2, x_3 due to the isotropy of the one-particle-matrix system, induced by the stresses, σ_{m1} and σ_{m2}, constant on the plane perpendicular to the axis x_1, representing integrals of w_{σ_m} over the surfaces $P_2P_3P_4$ and $P_1P_2P_4P_5$ for $x_1\langle 0, R\rangle$ and $x_1\langle R, R_c\rangle$, respectively, have the forms

$$\begin{aligned} W_{s\sigma_{m1}} &= \int_{S_m} w_{\sigma m}\,\mathrm{d}S_m \\ &= \frac{11m\sigma^2}{2}\left(R_c^2 - R^2\right), \quad x_1\langle 0, R\rangle, \quad R_c \to \infty, \end{aligned} \tag{109}$$

$$\begin{aligned} W_{s\sigma_{m2}} &= \int_{S_m} w_{\sigma m}\,\mathrm{d}S_m \\ &= \frac{11m\sigma^2}{2}\left(R_c^2 - x_1^2\right), \quad x_1\langle R, R_c\rangle, \quad R_c \to \infty. \end{aligned} \tag{110}$$

With regard to $R_c \to \infty$, the thermal-stress induced strengthening in the infinite matrix of the isotropic one-particle-matrix system, σ_{mi} (i = 1,2), derived from the condition, $W_{s\sigma_{mi}} = W_{smi}$, is derived as

$$\sigma_{mi} = 0, \tag{111}$$

and the thermal-stress induced strengthening in the spherical particle of the isotropic one-particle-matrix

system, σ_p, is given by Eq. 87, considering the particle-matrix boundary radial stress, p_b, derived by Eq. 93.

Application to SiC–Si_3N_4 multi-particle-matrix system

Compared to high strength and wear resistance, ceramic materials are characterized by low fracture toughness, usually strengthened by presence of particles of higher thermal expansion coefficient than that of a matrix. Increasing fracture toughness of the Si_3N_4 matrix by presence of the SiC particles of higher thermal expansion coefficient than that of the Si_3N_4 matrix, $\alpha_p > \alpha_m$ (Table 1), the SiC particle and the Si_3N_4 matrix are thus acted by the tensile thermal stresses, $\sigma_{rp} = \sigma = \sigma_{vp} = -p_b > 0$ (see Eqs. 11, 14) (see Fig. 21), and by tensile and compressive radial and tangential thermal stresses, $\sigma_{rm} > 0$ and $\sigma_{\varphi m} = \sigma_{vm} < 0$ (see Eqs. 12–14) (see Fig. 22), respectively.

Representing a resistance against tensile mechanical loading, the tensile radial thermal stress $\sigma_{rm} > 0$ in the Si_3N_4 cubic cell matrix, as a reason of the Si_3N_4 fracture toughness increase, and the compressive

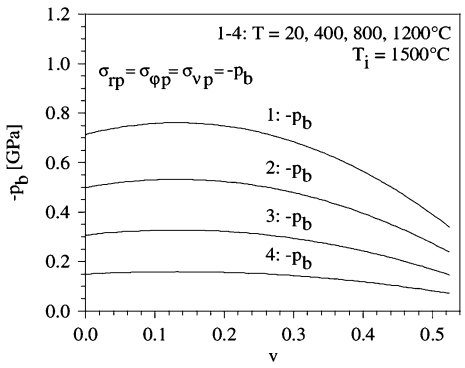

Fig. 21 The tensile radial and tangential thermal stresses in the SiC spherical particle, $\sigma_{rp} > 0$ and $\sigma = \sigma_{vp} > 0$, respectively, equal to the particle-matrix boundary radial stress, $-p_b$ (see Eqs. 4, 7), and the critical final temperature of a cooling process, T_c, as functions of the particle volume fraction, $v \in \langle 0, \pi/6)$, where T_i and T is the initial and final temperature of a cooling process, respectively. The $p_b - v$ dependence exhibits an extreme for the critical particle volume fraction $v_c = 0.132$

tangential radial stresses $\sigma_{\varphi m} = \sigma_{vm} < 0$, both decrease within the cubic cell matrix (see Fig. 22), the former from the maximal value on the particle-matrix boundary, $(\sigma_{rm})_{r=R} = -p_b$, where the particle-matrix boundary radial stress, $-p_b$, as a function of the particle volume fraction, $v \in \langle 0, \pi/6)$, exhibits the maximum for the critical particle volume fraction, $v_c = 0.132$ (see Fig. 21). Similarly, the tensile thermal stresses $\sigma_{rp} = \sigma_{\varphi p} = \sigma_{vp} = -p_b > 0$ in the SiC particle represents a resistance against compressive mechanical loading. Resulting from experimental results [11, 16], the SiC–Si_3N_4 multi-particle-matrix system exhibits a maximal fracture toughness for the SiC particle volume fraction, $v \approx 0.15$ [11, 16], corresponding to the calculated value, $v_c = 0.132$.

With regard to the yield stress in tension of the SiC particle, $\sigma_{ytp} = 1000$ MPa, and to the initial temperature of a cooling process, $T_i = 1500$ C [11, 16], the v-dependence of the critical final temperature of a cooling process, T_c (see Eq. 16), exhibits values <–273.15 °C in the interval $v \in \langle 0, \pi/6)$, and the presented derivations are thus considered in the temperature range $T \in \langle -273.15, 1500 \rangle$ C.

With regard to the material constants listed in Table 1 [11, 16], the dependences in Figs. 21, 22 and the following ones are generated on the condition of the linear T-dependence of the thermal expansion coefficient of the particle ($q = p$) and the matrix ($q = m$), α_q, derived the form

$$\alpha_q = \frac{\alpha_{q2}(T - T_1) - \alpha_{q1}(T - T_2)}{T_2 - T_1}, \tag{112}$$

where α_{q1} and α_{q2} are related to the temperature $T_1 = 20$ C and $T_2 = 1100$ C, respectively, for the particle volume fraction equal to critical, $v = v_c = 0.132$ (see Fig. 21), for the average SiC particle radius, $R = 250$ nm, consequently for the inter-particle distance, $d = 794$ nm, for the initial and different temperature of a cooling process, $T_i = 1500$ C and $T = 20, 400, 800, 1200$ C, respectively, and regarding the interval $v \in \langle 0, \pi/6)$, the formulae presented in the section 'Isotropic one-particle-matrix

Table 1 The material constants of the SiC particle and the Si_3N_4 matrix [11, 16, 18]

	E (GPa)	μ	α^a (10^{-6} K^{-1})	σ_{yt} (GPa)	σ_{yc} (GPa)	K_{IC} (MPa $m^{1/2}$)	R (nm)
SiC	360	0.19	4.14/5.05	1	5	3.25	10–500
Si_3N_4[b]	310	0.235	2.35/3.75	1	5	5.25	–

the Young's modulus, E; the Poisson's number, μ; the thermal expansion coefficient, α; the yield stress in tension and compression, σ_{yt} and σ_{yc}, respectively; the fracture toughness, K_{IC}; the SiC particle radius and volume fraction, R and v, respectively

[a] 20 °C/1,100 °C

[b] v = 0.05–0.3

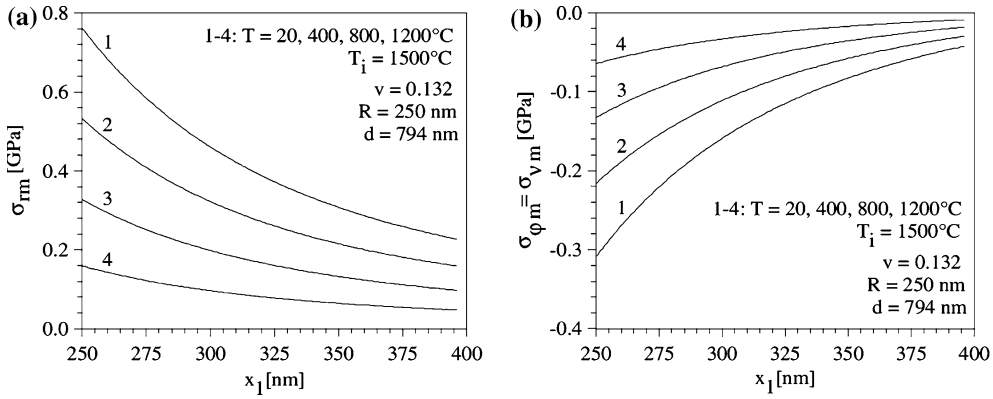

Fig. 22 The tensile radial (*a*) and compressive tangential (*b*) thermal stresses in the Si_3N_4 cubic cell matrix, $\sigma_{rm} > 0$ and $\sigma_{\varphi m} = \sigma_{\nu m} < 0$ (see Eqs. 5–7), respectively, as functions of the position $r = x_1 \in \langle R, d/2 \rangle$ (see Figs. 3–5), for the particle volume fraction equal to critical, $v = v_c = 0.132$ (see Fig. 21), where T_i and T is the initial and final temperature of a cooling process, respectively; R is the particle radius; and d is the inter-particle distance

system' are considered for $v = 0$. Furthermore, the v-dependences of the investigated parameters also result from the fact that a real multi-particle-matrix system is characterized by different local v, as a consequence of aperiodically distributed particles of different dimensions.

Resulting from the tensile thermal stresses in the SiC particle and consequently with regard to the particle crack formation, the SiC particle radius can be varied within the intervals, $R \in (0, R_{p1})$ and $R \in (0, R_{p2})$, for $v \in \langle 0, v_0 \rangle$ and $v \in \langle v_0, \pi/6 \rangle$ (see Fig.23a), where R_{p1} and R_{p2} (see Eqs. 30, 31) are reasons of the particle crack formation from the particle centre, O, to the particle surface, and vice versa (see Figs. 8, 9), respectively, and $v_0 = 0.487$. In addition, Fig. 23b shows the T-dependence of $R_{p0} = (R_{p1})_{v=v_0} = (R_{p2})_{v=v_0}$ for $v = v_0$, as a reason of the particle crack formation simultaneously from the particle centre, O, and the particle surface (see Fig. 10).

Although, the critical particle radii, R_{p1}, R_{p2}, are extremely high compared to the SiC particle radius of the interval, $R \in \langle 10, 500 \rangle$ nm, as an illustration, Fig. 24 shows the function, f_p (see Eq. 33), describing the particle crack shape in the interval $x_1 \in \langle 0, r_p \rangle$, in the form

$$f_p = 3.993 \times 10^{-5} - 1.568x_1 + 3.694 \times 10^{7}x_1^3 + 6.684 \times 10^{15}x_1^5 + 8.947 \times 10^{22}x_1^7 + 1.21 \times 10^{32}x_1^9 + 1.067 \times 10^{40}x_1^{11} \ldots \quad (113)$$

and accordingly the contribution of the term x_1^n for $n \geq 3$ is neglecting, where $r_p = 25.94\,\mu$m is derived from Eq. 32 by a numerical method for $v = v_c = 0.132$, $R_{p1} = 49.7\,\mu$m, $R = 55\,\mu$m. The quasi-linear shape

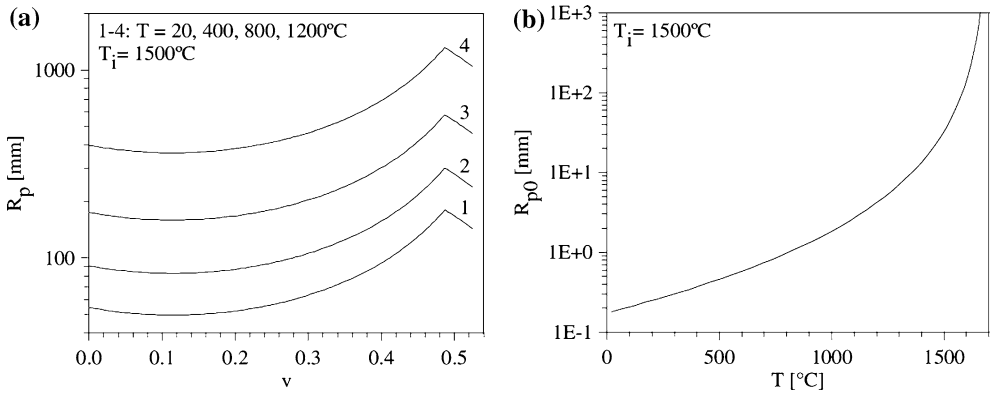

Fig. 23 The critical SiC particle radii, R_{p1} and R_{p2} (**a**) (see Eqs. 23, 24), as functions of the particle volume fraction, $v \in \langle 0, v_0 \rangle$ and $v \in \langle v_0, \pi/6 \rangle$, respectively, and the critical SiC particle radius, $R_{p0} = (R_{p1})_{v=v_0} = (R_{p2})_{v=v_0}$ (**b**), as a function of the final temperature of a cooling process, $T \in \langle 20, 1500 \rangle$ C for $v_0 = 0.487$, where T_i is the initial temperature of a cooling process

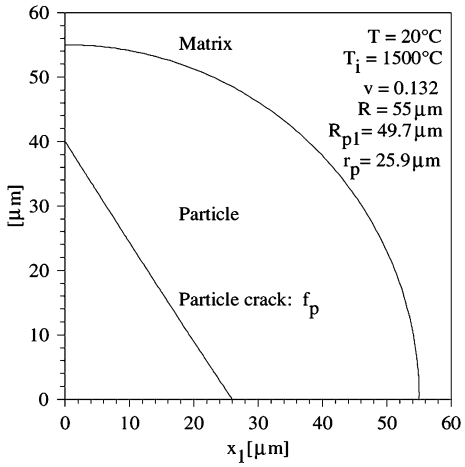

Fig. 24 The function, f_p, describing the SiC particle crack in the interval $x_1 \in \langle 0, r_p \rangle$ (see Eqs. 25, 26, 29) for the particle volume fraction equal to critical, $v = v_c = 0.132$ (see Fig. 21), and for the SiC particle radius, $R > (R_{p1})_{v=v_c}$ (see Fig. 23), where T_i and T is the initial and final temperature of a cooling process, respectively

corresponds to that from experimental results [4, 5, 11, 16].

If a magnetic domain wall or a dislocation move from the cubic cell surface to the particle-matrix boundary, the elastic energy gradient within the SiC–Si_3N_4 cubic cell, $W_s = W_{sp} + W_{sm1} + W_{sm2}$ (see Eqs. 81–84), as an increasing function of $x_1 \langle 0, d/2 \rangle$ (Fig. 25), and the maximum for $x_1 = 0$, W_{smax} (see Eqs. 85, 108), as a function of the spherical particle volume fraction $v \in \langle 0, \pi/6 \rangle$, exhibiting the maximum for $v = 0.096$ (Fig. 25d), represent a copybook shape of an energy barrier (Fig. 25c) [11] and its height, respectively, influencing magnetic domain and dislocation structure [11]. The elastic energy gradient, W_{sm2}, derived in the interval $x_1 \langle R, d/2 \rangle$ by Eqs. 83 and 84 exhibits identical courses. With regard to $W_{smax} \propto R^2$, the v-dependence of W_{smax} is related to the spherical particle radius $R = 1$.

The elastic energy gradients, W_{sm1} and W_{sm2}, correspond to thermal-stress induced strengthening within the Si_3N_4 cubic cell matrix, σ_{m1} and σ_{m2}, in the intervals $x_1 \in \langle 0, R \rangle$ and $x_1 \in \langle R, d/2 \rangle$ (see Eqs. 87–89) (Fig. 26), respectively. The thermal-stress induced strengthening in the SiC spherical particle, σ_p (see Eq. 87), and the average thermal-stress induced strengthening in the Si_3N_4 cubic cell matrix, $\overline{\sigma}_m$ (see Eq. 90), as functions of the spherical particle volume fraction, $v \in \langle 0, \pi/6 \rangle$, are presented in Fig. 27, where $|\sigma_p|$ exhibits the maximum for $v = v_c = 0.132$, and $\overline{\sigma}_m$ is independent on the parameter R, as resulted from the integration in Eq. 90) by a numerical method. With regard to $\alpha_m < \alpha_p$, the parameters, σ_{m1}, σ_{m2} and $\overline{\sigma}_m$, represent micro- and macro-strengthening against tensile mechanical loading, respectively. The $\overline{\sigma}_m - v$ dependence for the SiC–Si_3N_4 multi-particle-matrix system is in a good

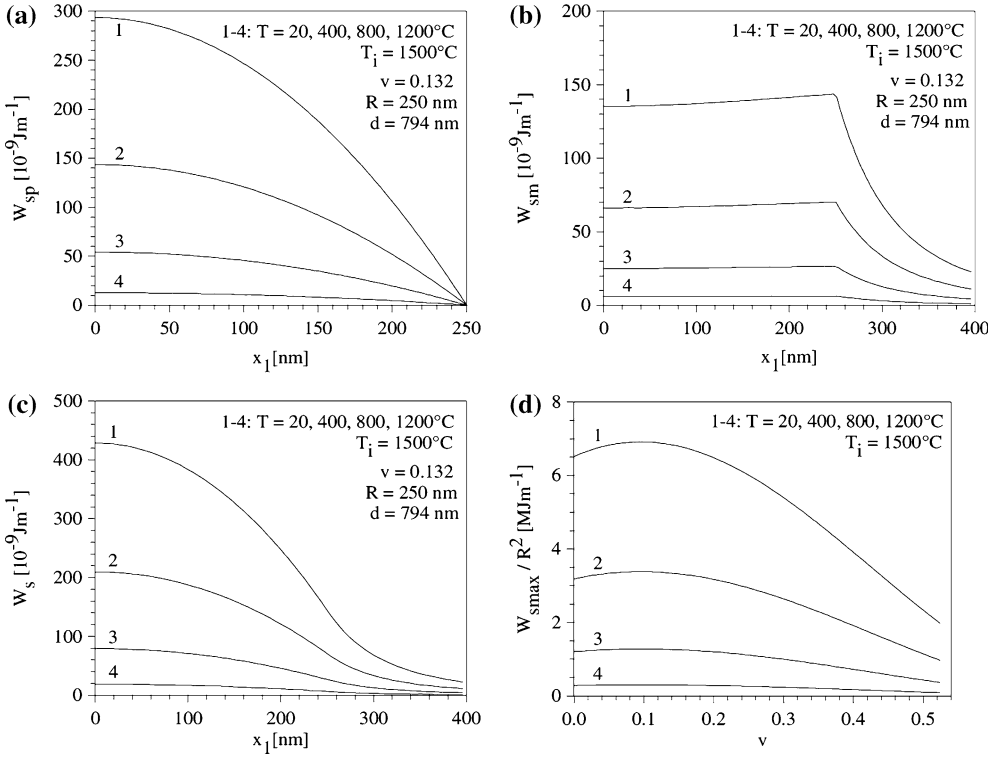

Fig. 25 The elastic energy gradient of the thermal stresses in the SiC spherical particle and the Si_3N_4 cubic cell matrix, W_{sp} (**a**) and W_{sm1}, W_{sm2} (**b**), as functions of the position $x_1 \in \langle 0, R \rangle$ and $x_1 \in \langle 0, R \rangle$, $x_1 \in \langle R, d/2 \rangle$ (Fig. 3), respectively, along with the elastic energy gradient of the thermal stresses in the SiC–Si_3N_4 cubic cell, $W_s = W_{sp} + W_{sm1} + W_{sm2}$ (**c**). The maximum of the elastic energy gradient of the thermal stresses in the SiC–Si_3N_4 cubic cell, W_{smax}/R^2, as a function of the spherical particle volume fraction, $v \in \langle 0, \pi/6 \rangle$ (**d**)

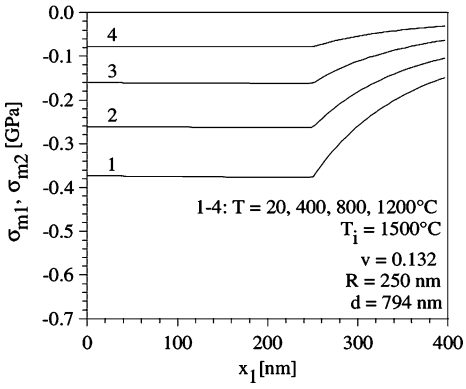

Fig. 26 The thermal-stress micro-strengthening in the Si_3N_4 cubic cell matrix, σ_{m1} and σ_{m2}, as functions of the position $x_1 \in \langle 0, R\rangle$ and $x_1 \in \langle R, d/2\rangle$ (Fig. 3), respectively

agreement with experimental results adverting to the tensile strength increase in the range $\Delta R_m = 0.3$–0.35 GPa for $v \approx 0.15$ and $T = 20\,\mathrm{C}$ [11, 16].

Conclusions

The paper is the continuation of derivations published in [13, 15], presenting the thermal stresses in the isotropic multi- and one-particle-matrix systems, respectively, originating during a cooling process as a consequence of the difference of thermal expansion coefficients between the particle and the matrix. The isotropic multi- and one-particle-matrix systems are represented by the periodically distributed spherical particles embedded in the infinite matrix imaginarily divided into cubic cells, containing one central particle [13], and by one spherical particle embedded in the infinite matrix [15], respectively.

Contributed to the results published in [13, 15] (see subsections 'Thermal stresses'), results of the presented derivations related to isotropic multi- and one-particle-matrix systems are as follows:

– The initial and critical final temperature of a cooling process between which the isotropic multi-particle-matrix systems are acted by elastic thermal stresses are derived (see subsections 'Temperature range of cooling process').
– The thermal-stress induced elastic energy density in a point, and along a curve in the spherical particle, in the cubic cell matrix and in the infinite matrix of the isotropic multi-particle-matrix systems are derived (see subsections 'Elastic energy density', 'Curve integral of elastic energy density').
– Resulting from the 'curve' elastic energy density, the subsections 'Particle and matrix crack initiation and formation', devoted to the particle crack formation include

  - the condition concerning a direction of the crack formation in the spherical particle of the isotropic multi-particle-matrix systems is derived,
  - the critical particle radii, as a reason of the crack formation in the spherical particle of the isotropic multi-particle-matrix system are derived,
  - the functions describing cracks in the spherical particle of the isotropic multi-particle-matrix systems are derived.

– The thermal-stress induced elastic energy density on a surface in the spherical particle, in the cubic cell matrix and in the infinite matrix of the isotropic particle-matrix systems are derived (see subsections 'Surface integral of elastic energy density').
– Resulting from the 'surface' elastic energy density, the thermal-stress induced strengthening in the spherical particle, in the cubic cell matrix and in the infinite matrix of the isotropic particle-matrix systems are derived (see subsections 'Particle and matrix thermal-stress induced strengthening').

Applying the derived formulae to the SiC–Si_3N_4 multi-and one multi-particle-matrix systems, the main results included in the section 'Application to SiC–Si_3N_4 multi-particle-matrix system' are as follows:

– The SiC spherical particle thermal stresses, the particle-matrix boundary radial stress and the critical final temperature of a cooling process, as functions of the particle volume fraction, v, are presented (see Fig. 21).
– The critical SiC particle volume fraction, $v_c = 0.132$ (see Fig. 21), corresponding to maximal calculated thermal stresses, is in an excellent agreement with the SiC particle volume fraction, $v \approx 0.15$, corresponding to a maximal fracture toughness as obtained from published experimental results [11, 16].
– The thermal stresses, as functions of the position in the Si_3N_4 cubic cell matrix, are presented for the $v = v_c = 0.132$ and for the average SiC particle radius, $R = 250$ nm (see Fig. 22).
– The critical SiC particle radii, as reasons of the SiC particle crack formation and as functions of v, are presented along with the temperature dependence of the SiC critical particle radius (see Fig. 23).
– The function describing the particle crack for the critical particle volume fraction and for the SiC particle radius greater than critical is presented (see Fig. 24).
– The thermal-stress induced elastic energy gradient, as a function of the position in the SiC–Si_3N_4 cubic

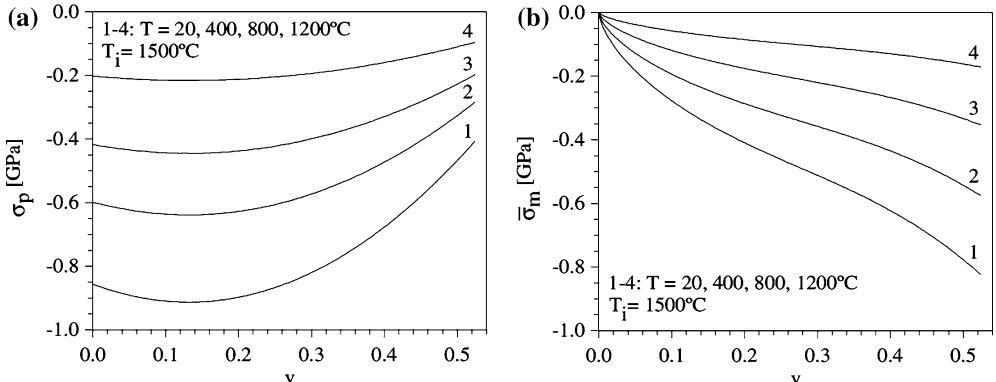

Fig. 27 The thermal-stress induced macro-strengthening in the SiC spherical particle, σ_p, and the average thermal-stress induced strengthening in the Si_3N_4 cubic cell matrix, $\overline{\sigma}_m$, as functions of the spherical particle volume fraction, $v \in \langle 0, \pi/6)$

cell, is presented (Fig. 25a, b, c) along with the v-dependence of the gradient maximum (Fig. 25d).

– The thermal-stress induced strengthening, as a function of the position in the Si_3N_4 cubic cell matrix, is presented (Fig. 26) along with the v-dependences of the thermal-stress induced strengthening in the SiC spherical particle and the average thermal-stress induced strengthening in the Si_3N_4 cubic cell matrix (Fig. 27), being in a good agreement with published experimental results [11, 16].

Acknowledgements This work was supported by the Slovak Grant Agency VEGA (2/7197/27, 2/7194/27, 2/7195/27), by NANOSMART, Centre of Excellence, Slovak Academy of Sciences, by Science and Technology Assistance Agency under the contract No. APVV-20-061505, APVV-20-024405, by RTN2-2001-00488 SICMAC, by 2003 SO 51/03R8 06 00/03R 06 03-2003, by EU 5th FP project No. GRD1-2000-25352 "SmartWeld", by COST Action 536 and COST Action 538, by T043704 OTKA foundation, by János Bolyai Research Grant NSF-MTA-OTKA grant MTA: 96/OTKA: 049953.

Author is thankful to his dearest parents for their support.

Appendix

The elastic moduli of the particle ($q = p$) and the matrix ($q = m$), s_q, have the forms

$$s_{11q} = \frac{1}{E_q}, \tag{114}$$

$$s_{12q} = -\frac{\mu_q}{E_q}, \tag{115}$$

where E_q and μ_q are the Young's modulus and Poisson's number, respectively.

The coefficient c is derived as

$$c_1 = \frac{3\pi(s_{11m} + s_{12m})}{2(\pi - 6v)}, \tag{116}$$

$$c_2 = c_1 + s_{11p} + 2s_{12p} - (s_{11m} + 2s_{12m}), \tag{117}$$

$$c_3 = \int_0^{\pi/4} \left[\frac{\cos^4\varphi}{\sqrt{1+\cos^2\varphi}} - \frac{1}{3}\left(\frac{\cos^2\varphi}{\sqrt{1+\cos^2\varphi}} \right)^3 \right] \mathrm{d}\varphi, \tag{118}$$

where the coefficient c_3 can be derived by the Taylor series for the integrated function. Consequently, after integration of the Taylor series in terms of $(\varphi - \varphi_0)^n$ about the point $\varphi_0 = 0$, the coefficient $c_3 = 0.337497$ for $n = 100$;

$$\begin{aligned} c_4 =& 2v(s_{11p} + 2s_{12p})\left(\frac{c_1}{c_2}\right)^2 \\ &+ \frac{1}{(\pi - 6v)^2}\left[2\pi^2(1-v)(s_{11m} + 2s_{12m})\left(1 - \frac{6vc_1}{\pi c_2}\right)^2 \right. \\ &\left. + v(s_{11m} - s_{12m})(\pi^2 - 36vc_3)\left(1 - \frac{c_1}{c_2}\right)^2 \right], \end{aligned} \tag{119}$$

$$\begin{aligned} c_5 =& \frac{2c_1(s_{11p} + 2s_{12p})}{c_2} \\ &+ \frac{1}{(\pi - 6v)^2}\left[12\pi(1-v)(s_{11m} + 2s_{12m})\left(1 - \frac{6vc_1}{\pi c_2}\right) \right. \\ &\left. + (s_{11m} - s_{12m})(\pi^2 - 36vc_3)\left(1 - \frac{c_1}{c_2}\right) \right], \end{aligned} \tag{120}$$

$$c_6 = \frac{\pi[c_2c_4 + vc_5(c_1 - c_2)]}{(\pi - 6v)(c_2c_4 + vc_1c_5)}, \tag{121}$$

$$c_7 = \frac{c_2c_4 + \nu c_1c_5}{c_2^2c_4}, \tag{122}$$

$$c_8 = \frac{\nu[\pi c_2c_5 - 6(c_2c_4 + \nu c_1c_5)]}{(\pi - 6\nu)(c_2c_4 + \nu c_1c_5)}, \tag{123}$$

$$\begin{aligned} c_9 = {} & \Big\{5\nu^2(s_{11m} + 2s_{12m})[c_5(6\nu c_1 - \pi c_2) + 6c_2c_4]^2 \\ & -(s_{11p} + 2s_{12p})(\pi - 6\nu)^2(c_2c_4 + \nu c_1c_5)^2\Big\} \\ & + 16\pi^2(s_{11m} - s_{12m})[\nu c_5(c_1 - c_2) + c_2c_4]^2 \\ & \times \left(\frac{3\nu}{4\pi}\right)^{5/3}\left\{1 - \left[\frac{(4\pi)^{1/3}}{\sqrt{(4\pi)^{2/3} + 4(3\nu)^{2/3}}}\right]^5\right\}, \end{aligned} \tag{124}$$

$$c_{10} = s_{11p} + 2s_{12p} + \frac{1}{2}(s_{11m} - s_{12m}), \tag{125}$$

$$c_{11} = \frac{3\pi + 8}{2R^4}\left(\frac{3\nu}{4\pi}\right)^{4/3}, \quad x_1 = 0, \tag{126}$$

$$\begin{aligned} c_{11} = {} & \int_0^{\pi/4}\left[\frac{4(3\nu)^{2/3}\cos^2\xi}{R^2(4\pi)^{2/3} + 4x_1(3\nu)^{2/3}\cos^2\xi}\right]^2 \mathrm{d}\xi, \\ & x_1 \in \left\langle 0, \frac{d}{2}\right\rangle, \end{aligned} \tag{127}$$

where the coefficient c_{11} for $x_1 \in \langle 0, d/2\rangle$ can be derived for a concrete isotropic particle-matrix system by the Taylor series for the integrated function in terms of $(\xi - \xi_0)^n$ about the point $\xi_0 = 0$;

$$c_{12} = 3\varphi_{73} + \frac{2x_1R(12\pi\nu)^{1/3}\left[3R^2(4\pi)^{2/3} + 20x_1^2(3\nu)^{2/3}\right]}{\left[R^2(4\pi)^{2/3} + 4x_1^2(3\nu)^{2/3}\right]^2}, \tag{128}$$

$$c_{13} = \int_0^{\varphi_{73}} v_6\cos^4\varphi\,\mathrm{d}\varphi, \tag{129}$$

$$\begin{aligned} c_{14} = {} & \int_0^{\varphi_{22}} \frac{R^4(4\pi)^{4/3}\cos^5\varphi}{\left[R^2(4\pi)^{2/3}\cos^2\varphi + 4x_1^2(3\nu)^{2/3}\right]^2}\,\mathrm{d}\varphi \\ = {} & \frac{R(4\pi)^{1/3}}{\sqrt{R^2(4\pi)^{2/3} + 4x_1^2(3\nu)^{2/3}}}\left\{\frac{R^2(4\pi)^{2/3} + 3x_1^2(3\nu)^{2/3}}{R^2(4\pi)^{2/3} + 2x_1^2(3\nu)^{2/3}}\right. \\ & - \left(\frac{2x_1}{R}\right)^2\left(\frac{3\nu}{4\pi}\right)^{2/3}\frac{R^2(4\pi)^{2/3} + 3x_1^2(3\nu)^{2/3}}{R^2(4\pi)^{2/3} + 4x_1^2(3\nu)^{2/3}} \\ & \left.\times\ln\left[1 + \frac{1}{2}\left(\frac{R}{x_1}\right)^2\left(\frac{4\pi}{3\nu}\right)^{2/3}\right]\right\}, \end{aligned} \tag{130}$$

$$\begin{aligned} c_{15} = {} & \int_0^{\varphi_{73}} \frac{R^2(4\pi)^{2/3}\cos^5\varphi}{R^2(4\pi)^{2/3}\cos^2\varphi + 4x_1^2(3\nu)^{2/3}}\,\mathrm{d}\varphi \\ = {} & \frac{(3\nu)^{1/3}}{\sqrt{R^2(4\pi)^{2/3} + 4x_1^2(3\nu)^{2/3}}}\left\{\frac{R^2(4\pi)^{2/3} - 4x_1^2(3\nu)^{2/3}}{R(12\pi\nu)^{1/3}}\right. \\ & - \frac{4\pi R^3}{3(3\nu)^{1/3}\left[R^2(4\pi)^{2/3} + 4x_1^2(3\nu)^{2/3}\right]} \\ & \left. + \frac{6\nu x_1^4}{\pi R^3}\ln\left[1 + \frac{1}{2}\left(\frac{R}{x_1}\right)^2\left(\frac{4\pi}{3\nu}\right)^{2/3}\right]\right\}, \end{aligned} \tag{131}$$

$$\begin{aligned} c_{16} = {} & \int_0^{\varphi_{73}} \frac{(4\pi)^{4/3}R^4\cos^7\varphi}{\left[R^2(4\pi)^{2/3}\cos^2\varphi + 4x_1^2(3\nu)^{2/3}\right]^2}\,\mathrm{d}\varphi \\ = {} & \frac{1}{\sqrt{R^2(4\pi)^{2/3} + 4x_1^2(3\nu)^{2/3}}}\left\{\frac{R^2(4\pi)^{2/3} - 8x_1^2(3\nu)^{1/3}}{R(4\pi)^{1/3}}\right. \\ & + 3R^4(4\pi)^{4/3} - 16x_1^4(3\nu)^{4/3}4R(4\pi)^{1/3} \\ & \left[R^2(4\pi)^{2/3} + 2x_1^2(3\nu)^{2/3}\right] \\ & - \frac{4\pi R^3}{3\left[R^2(4\pi)^{2/3} + 4x_1^2(3\nu)^{2/3}\right]} \\ & + \frac{2R^5(4\pi)^{5/3}\left[R^4(4\pi)^{4/3} - 6x_1^4(3\nu)^{4/3}\right]}{\left[R^2(4\pi)^{2/3} + 4x_1^2(3\nu)^{2/3}\right]^4} \\ & \left.\times\ln\left[1 + \frac{1}{2}\left(\frac{R}{x_1}\right)^2\left(\frac{4\pi}{3\nu}\right)^{2/3}\right]\right\}, \end{aligned} \tag{132}$$

$$\begin{aligned} c_{17} = {} & \frac{2x_1}{R}\left(\frac{3\nu}{4\pi}\right)^{1/3}\left[c_{14}\left(\frac{2x_1}{R}\right)^2\left(\frac{3\nu}{4\pi}\right)^{2/3} + 4c_{15} - c_{16}\right] \\ & + \frac{3\pi c_{12}}{16} - 3c_{13}, \end{aligned} \tag{133}$$

where the coefficient c_{13} can be derived for a concrete isotropic particle-matrix system by the Taylor series for the integrated function in terms of $(\varphi - \varphi_0)^n$ about the point $\varphi_0 = 0$;

$$\varphi_{73} = \arctan\left[\frac{R}{2x_1}\left(\frac{4\pi}{3\nu}\right)^{1/3}\right], \tag{134}$$

$$v_6 = \arctan\left[\frac{2x_1}{R\cos\varphi}\left(\frac{3\nu}{4\pi}\right)^{1/3}\right], \tag{135}$$

$$c_{18} = \frac{s_{11m}}{2}\left[R^2\left(\frac{4\pi}{3v}\right)^{2/3} - \pi\left(R^2 - x_1^2\right)\right], \quad x_1 \in \langle 0, R\rangle, \tag{136}$$

$$c_{19} = \frac{s_{11m}R^2}{2}\left(\frac{4\pi}{3v}\right)^{2/3}. \tag{137}$$

References

1. Ivančo V, Kubín K, Kostolný K (1994) In: Finite element method I. Elfa, Košice, Slovak Republic, p 36 (in Slovak)
2. Hvizdoš P, Lofaj F, Dusza K (1995) Metall Mater 33:473
3. Besterci M, Velgošová O, Lofaj F (2003) Acta Mech Slovaca 4:47
4. Diko P (1998) Supercond Sci Technol 11:68
5. Diko P (1998) Mater Sci Eng B 83:149
6. Janovec J, Magula V, Holý A, Výrostková A (1992) Scripta Metall Mater 26:1303
7. Janovec J, Výrostková A, Svoboda M (1994) Metall Mater Trans A25:267
8. Sidor Y, Kováč F, Novák L, Kravčák (2002) J Acta Electrotech Inform 2(3):96
9. Sidor Y, Kováč F, Petrychka V (2004) Acta Metall Slovaca 10:698
10. Petrychka V, Kováč F, Sidor Y (2004) Acta Metall Slovaca 10:702
11. Skočovský P, Bokůvka O, Konečná R, Tillová E (2001) In: Science on materials for mechanical engineers. EDIS Technical University in Žilina, Žilina, Slovak Republic, p 252 (in Slovak)
12. Mizutani T (1996) J Mater Res 11:483
13. Ceniga L (2004) J Thermal Stresses 27:425
14. Ceniga L (2005) In: Caruta BM (ed) New developments in material science research. Nova Science Publishers, New York, USA, ISBN: 1-59454-793-9
15. Ceniga L, Kováč F (2001) Mater Sci Eng B86:178
16. Pánek Z, Figusch V, Haviar M, Ličko T, Šajgalík P, Dusza J (1992) In: Structural ceramics. R&D. Bratislava, Slovak Republic, p 27 (in Slovak)
17. Kluvánek I, Mišík L, Švec M (1959) In: Mathematics I. Alfa, Bratislava, Slovak Republic, p 685 (in Slovak)
18. Zimovčák P, Köves T, Dusza J, Chalvet F, Portu G (2005) Key Mater Eng 290:264